The International Journal of
Robotics Research
31(9) 1094–1113

DOI: 10.1177/0278364912452673
ijr.sagepub.com

Capturability-based analysis and control of legged locomotion, Part 1: Theory and application to three simple gait models

Twan Koolen[1,2], Tomas de Boer[2], John Rebula[3], Ambarish Goswami[4] and Jerry Pratt[1]

Abstract

This two-part paper discusses the analysis and control of legged locomotion in terms of N-step capturability: the ability of a legged system to come to a stop without falling by taking N or fewer steps. We consider this ability to be crucial to legged locomotion and a useful, yet not overly restrictive criterion for stability. In this part (Part 1), we introduce a theoretical framework for assessing N-step capturability. This framework is used to analyze three simple models of legged locomotion. All three models are based on the 3D Linear Inverted Pendulum Model. The first model relies solely on a point foot step location to maintain balance, the second model adds a finite-sized foot, and the third model enables the use of centroidal angular momentum by adding a reaction mass. We analyze how these mechanisms influence N-step capturability, for any $N > 0$. Part 2 will show that these results can be used to control a humanoid robot.

Keywords

Legged robots, push recovery, viability, capturability, capture points.

1. Introduction

Preventing falls is essential in legged locomotion. A fall can be energetically costly and dangerous for both the legged system itself and other agents. Healthy humans are able to avoid falling in almost all conditions experienced in everyday life. While many legged robots can currently walk, run, and dance without falling, these tasks are usually performed in a controlled environment. Unexpected perturbations will easily topple most current bipedal robots. The ability of legged robots to avoid falling must be significantly improved before they can find utility in complex environments.

Measuring how close a legged system is to falling can provide useful insight and could be used for controller design. However, effectively quantifying closeness to falling is challenging. For traditional control systems, stability can be analyzed using measures such as eigenvalues, phase margins or loop gain margins. Legged locomotion on the other hand is generally characterized by nonlinear dynamics, under-actuation, and a combination of continuous and discrete dynamics. These properties limit the relevance of traditional analysis and control techniques to legged locomotion.

Existing stability measures for legged locomotion such as those based on the zero moment point (ZMP) or a Poincaré map analysis may be readily computed but only apply to specific classes of controllers or robot motions (Masani et al. 2006; Hobbelen and Wisse 2007a). More general techniques, such as the viability margin (Wieber 2002), have been proposed but are difficult to compute, limiting their usefulness.

This leads us to propose the analysis of legged locomotion based on N-step capturability, which we informally define as the ability of a system to come to a stop without falling by taking N or fewer steps, given its dynamics and actuation limits. N-step capturability offers measures that are applicable to a large class of robot motions, including non-periodic locomotion over rough terrain with impassable regions, and it does not require a specific control system design. N-step capturability may be readily approximated, and it is useful in controller design.

Both preventing a fall and coming to a stop require adequate foot placement as a result of the ground reaction force constraints that are typical to legged locomotion. We focus extensively on this aspect of legged locomotion using the N-step capture region, the set of points to which a legged system in a given state can step to become

[1]Institute for Human and Machine Cognition, Pensacola, FL, USA
[2]Delft University of Technology, the Netherlands
[3]University of Michigan, Ann Arbor, MI, USA
[4]Honda Research Institute, Mountain View, CA, USA

Corresponding author:
Twan Koolen, Institute for Human and Machine Cognition, 40 South Alcaniz Street, Pensacola, FL 32502, USA.
Email: tkoolen@ihmc.us

($N-1$)-step capturable. A new measure of capturability in a given state, termed the N-step capturability margin, is then naturally defined as the size of the N-step capture region. Additionally, we will introduce the d_∞ capturability level, which allows a general, state-independent capturability comparison between simple gait models.

The remainder of this first part is structured as follows. Section 2 provides a survey of relevant literature. Section 3 contains definitions of the various concepts that constitute the N-step capturability framework. In Sections 4–7 we apply the capturability framework to three simple gait models based on the Linear Inverted Pendulum Model (Kajita and Tanie 1991; Kajita et al. 2001). For these simple gait models, we can exactly compute capturability. Section 8 introduces the two capturability measures and compares the simple gait models in terms of these measures. A discussion is provided in Section 9, and we conclude the part in Section 10.

In Part 2 of the paper (Pratt et al. 2012), we demonstrate the utility of the capturability framework by using the results of the simple gait models to control and analyze balancing and walking motions of a 3D bipedal robot with two 6-degree-of-freedom (6-DoF) legs.

2. Background

The question 'how stable is a given legged system?' has been the subject of much research and debate, in both robotics and biomechanics. We now present previous work attempting to answer this question, including previous work on capturability.

The ZMP is often used as an aid in control development, with the constraint that it must remain in the interior of the base of support of a legged robot. A common ZMP control method is to maintain the ZMP along a precomputed reference trajectory (Vukobratovic and Stepanenko 1972). During walking, the error between the actual and desired ZMP can be used as a measure of the error between the current and desired state of the robot (Okumura et al. 2003). The repeatability of the gait can also be used as an error measure (Vukobratovic and Stepanenko 1972). One drawback to following a precomputed trajectory is the inability of the robot to recover from a large unexpected push. Further work has expanded the ZMP method to include step placement adjustment in reaction to disturbances (Morisawa et al. 2009; Nishiwaki and Kagami 2010), but there is no measure of the ability of the robot to reactively avoid a fall when following a given preplanned ZMP trajectory. In addition, the ZMP requires significant modification to apply to non-flat terrain (Wieber 2002) or dynamic gait with a foot that rotates on the ground.

Poincaré maps have been used to measure the local stability of periodic gaits, and to induce periodic gaits of real robots using reference trajectories (Morimoto et al. 2005). Based on Poincaré map analysis, the gait sensitivity norm (Hobbelen and Wisse 2007a) provides a measure of robustness for limit cycle walkers (Hobbelen and Wisse 2007b) and has been shown to correlate well with the disturbance rejection capabilities of simulated planar walkers. The gait sensitivity norm is calculated as the sensitivity of a given gait measure, such as step time, to a given disturbance type, such as a step-down in terrain, using a simulated model or experimental data. Another Poincaré map method based on Floquet multipliers has been used to analyze the stability of human walking gaits (Dingwell et al. 2001). However, Poincaré map analysis assumes cyclic gait to yield a measure of stability. In addition, it requires a linearization at a given point in the gait cycle, which limits the applicability of the method to large disturbances between steps where the linearization fails to capture essential dynamics of the motion (Dingwell et al. 2001).

Poincaré map analysis has also been applied to the case of passive limit cycle walkers under stochastic environmental perturbations (Byl and Tedrake 2008), without linearizing the system around the fixed point, yielding a probabilistic basin of attraction. The stability of a walker is described with a mean first passage time, which is the expected number of steps before failure, given a set of statistics for the stochastic environmental disturbance. However, this method assumes an approximately periodic gait, and does not apply to large general disturbances such as a significant push. Poincaré map analysis has been extended to control a walker in acyclic desired gaits, by applying linear control based on a continuous family of Poincaré maps along the entire trajectory (Manchester et al. 2009). This control method can provide a measure of robustness about the desired trajectory, but it does not consider the robustness of the desired trajectory itself.

The concepts of virtual constraints and hybrid zero dynamics have been used to obtain and prove asymptotic stability of periodic motions for walking robots (Chevallereau et al. 2003). Introducing virtual constraints reduces the dimensionality of the walking system under consideration by choosing a single desired gait, allowing a tractable stability analysis. However, if actuator limitations render the robot incapable of maintaining the virtual constraints after a large perturbation, it is possible a fall could be avoided only by changing the desired trajectory to alter foot placement and use of angular momentum.

The foot placement estimator, like the present work, considers the footstep location to be of primary importance and can be used both to control and to analyze bipedal systems (Wight et al. 2008). For a simple planar biped that maintains a rigid A-frame configuration, the foot placement estimator demarcates the range of foot placement locations that will result in a statically standing system. This approach is quite similar to ours, although it is unclear how to extend this method to more general systems.

Aubin used the concept of viability theory (1991) to reason about the subset of state space in which the legged system must be maintained to avoid falling (Weiber 2002).

A Lyapunov stability analysis was presented for standing on non-flat terrain given a balance control law. However, the standing assumption precludes the use of this method in walking, and it provides no information on choosing step locations to avoid falling. Capturability is closely related to viability theory, but focuses on states which are most relevant to normal walking and also provides a method to explicitly compute acceptable regions to step.

In previous work, we have implicitly used the concept of capturability to develop the notion of capture points, the places on the ground to step that will allow a legged robot to come to a stop. We have used capture points based on simple models to control complex models, including a simulation of M2V2, a 12-DoF humanoid robot. We have designed controllers that balance, recover from pushes, and walk across randomly placed stepping stones (Pratt and Tedrake 2006; Rebula et al. 2007). Some of these capture point-based control methods were also implemented on the physical M2V2 (Pratt and Krupp 2008). We extend the concept of capture points, applying the theory to general legged systems, considering multiple steps and providing a more complete analysis of the ability of a legged system to come to a stop.

3. Capturability framework

Consider a class of hybrid dynamic systems that have dynamics described by

$$\dot{\mathbf{x}} = \mathbf{f}(\mathbf{x}, \mathbf{u}) \qquad \text{if } h_i(\mathbf{x}) \neq 0 \tag{1a}$$

$$\mathbf{x} \leftarrow \mathbf{g}_i(\mathbf{x}) \qquad \text{if } h_i(\mathbf{x}) = 0 \tag{1b}$$

$$\mathbf{u} \in \mathbf{U}(\mathbf{x}) \tag{1c}$$

for $i \in I \subset \mathbb{N}$. Here, $\mathbf{x}$ is the state of the system and $\mathbf{u}$ is the system's control input, which is confined to the state-dependent set of allowable control inputs $\mathbf{U}(\mathbf{x})$. When the system state lies on a switching surface, such that $h_i(\mathbf{x}) = 0$ for some i contained in the switching surface index set I, the discrete jump dynamics reset the state to $\mathbf{g}_i(\mathbf{x})$ instantaneously. An evolution of this system is a solution to Equations (1a) and (1b) for some input satisfying (1c).

For this analysis, we assume that some part of state space must be avoided at all cost: a set of failed states. For a bipedal robot, this set could comprise all states for which the robot has fallen. The viability kernel, described by Aubin (1991); Aubin et al. (2002) and introduced into the field of legged locomotion by Wieber (2000, 2002), is the set of all states from which these failed states can be avoided. That is, for every initial state in the viability kernel, there exists at least one evolution that never ends up in a failed state. As long as the system state remains within the viability kernel, the system is viable.

The viability concept arises quite naturally and can be seen as a very generic and unrestrictive definition of 'stability' for a dynamic system. However, determining the viability kernel is generally analytically intractable, and approximation is computationally expensive (Wieber 2002). In addition, it is not trivial to synthesize a controller based solely on the viability kernel, even if it were given. This motivates the use of more restrictive definitions of stability. N-step capturability adds the restriction that the system be able to come to a stop by taking N or fewer steps, resulting in the following definition.

Definition 1 (N-step capturable)**.** *Let* $\mathbf{X}_{\text{failed}}$ *denote a set of failed states associated with a hybrid dynamic system defined by Equation* (1)*. A state* $\mathbf{x}_0$ *of this system is* N*-step capturable with respect to* $\mathbf{X}_{\text{failed}}$*, for* $N \in \mathbb{N}$*, if and only if there exists at least one evolution starting at* $\mathbf{x}_0$ *that contains* N *or fewer crossings of switching surfaces (steps), and never reaches* $\mathbf{X}_{\text{failed}}$*.*

Similar to the viability kernel and the viable-capture basin (Aubin et al. 2002), we define an N-step viable-capture basin as the set of all N-step capturable states. The 0-step viable-capture basin will also be referred to as the set of captured states, and if a system's state is within the 0-step viable-capture basin, the system will be referred to as captured.

N-step viable-capture basins, shown schematically in Figure 1, describe the subsets of state space in which a controller should maintain the system so that the system is able to reach a captured state ('come to a stop') by taking N or fewer steps. For $N > 0$, the N-step viable-capture basin is equivalent to the set containing every initial state $\mathbf{x}_0$ for which at least one evolution containing a single step and starting at $\mathbf{x}_0$ reaches the $(N-1)$-step viable-capture basin in finite time, while never reaching a failed state. This property allows the use of recursive methods to derive or approximate N-step viable-capture basins.

The ∞-step viable-capture basin is generally a strict subset of the viability kernel because having the ability to eventually come to a stop is not a necessary condition for avoiding the set of failed states. However, for human locomotion, the difference between the ∞-step viable-capture basin and the viability kernel is 'small', as it is hard to imagine a state in which a human can avoid falling, but cannot eventually come to a captured state. A notable exception is a purely passive walker (McGeer 1990), for which walking persists in an infinite limit cycle with no possibility of coming to a stop. In fact, an infinitely repeatable gait has been found for a simulated 3D passive walking model that has no captured states (Coleman et al. 2001).

A problem that N-step viable-capture basins share with the viability kernel is that they do not provide a direct means of controller design. This motivates the introduction of N-step capture points and N-step capture regions. While viable-capture basins specify capturability in terms of state space, capture points and capture regions are defined in Euclidean space, and describe the places where the system can step to reach a captured state. This information can, for example, be used to determine future step locations, to be used in a control algorithm for a bipedal robot.

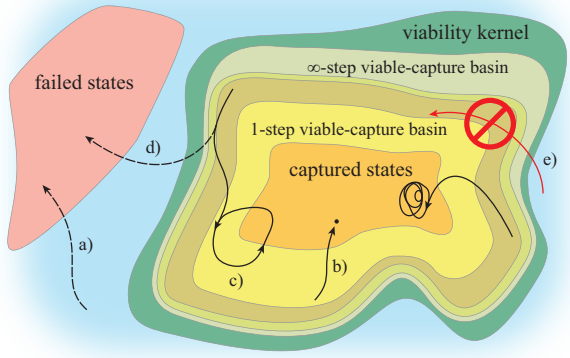

Fig. 1. Conceptual view of the state space of a hybrid dynamic system. Several N-step viable-capture basins are shown. The boundary between two N-step viable-capture basins is part of a step surface. The ∞-step viable-capture basin approximates the viability kernel. Several evolutions are shown: (a) an evolution starting outside the viability kernel inevitably ends up in the set of failed states; (b) the system starts in the 1-step viable-capture basin, takes a step, and comes to a rest at a fixed point inside the set of captured states (i.e. the 0-step viable-capture basin); (c) an evolution that eventually converges to a limit cycle; (d) an evolution that has the same initial state as (c), but ends up in the set of failed states because the input $\mathbf{u}(\cdot)$ was different; (e) impossible evolution: by definition, it is impossible to enter the viability kernel if the initial state is outside the viability kernel.

We encode step locations using contact reference points. Each body that is allowed to come into contact with the environment during normal operation is assigned a single contact reference point, which is fixed with respect to the contacting body. Contact reference points provide a convenient, low-dimensional way of referring to the position of a contacting body, and allow us to define the N-step capture points and N-step capture regions as follows.

Definition 2 (N-step capture point, region)**.** *Let* $\mathbf{x}_0$ *be the state of a hybrid dynamic system defined by* (1)*, with an associated set of failed states* $\mathbf{X}_{failed}$*. A point* $\mathbf{r}$ *is an N-step capture point for this system, for* $N > 0$*, if and only if there exists at least one evolution starting at* $\mathbf{x}_0$ *that contains one step, never reaches* $\mathbf{X}_{failed}$*, reaches an* $(N-1)$*-step capturable state, and places a contact reference point at* $\mathbf{r}$ *at the time of the step.*

The N-step capture region is the set of all N-step capture points.

A conceptual visualization of N-step capture regions is shown in Figure 2.

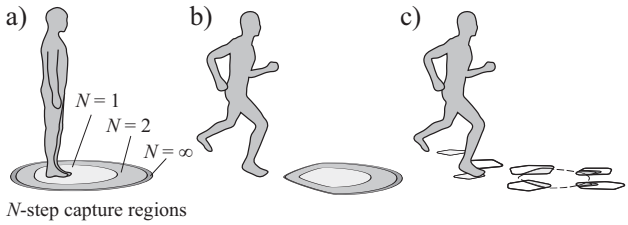

Fig. 2. (a) A conceptual representation of the N-step capture regions for a human in a captured state (standing at rest). (b) N-step capture regions for a running human. The capture regions have decreased in size and have shifted, as compared with (a). (c) N-step capture regions for the same state as (b), but with sparse footholds (e.g. stepping stones in a pond). The set of failed states has changed, which is reflected in the capture regions.

4. Three simple gait models

Legged locomotion can be difficult to analyze and control due to the dynamic complexity of a legged system. Simple gait models permit tractable and insightful analysis and control of walking. We present three models for which it is possible to determine N-step viable-capture basins and capture regions in closed form. The results can be used as approximations for more complex legged systems and prove useful in their control.

To illustrate the results obtained in this research, a Matlab graphical user interface (GUI) was created that allows the user to manipulate the control inputs for all models described in this paper, while the N-step capture regions are dynamically updated. This GUI is included as Extension 1.

All three models are based on the 3D Linear Inverted Pendulum Model (3D-LIPM) (Kajita and Tanie 1991; Kajita et al. 2001), which comprises a single point mass maintained on a plane by a variable-length leg link. The complexity of the presented models increases incrementally. To each subsequent model, another stabilizing mechanism is added. These mechanisms are generally considered fundamental in dealing with disturbances, both in the biomechanics and robotics literature (Horak and Nashner 1986; Guihard and Gorce 2002; Abdallah and Goswami 2005; Hyon et al. 2007; Stephens 2007b; Nenchev and Nishio 2008).

The first model (Section 5) relies solely on point foot placement to come to a stop. The second model (Section 6) is obtained by adding a finite-sized foot and ankle actuation to the first model, enabling modulation of the center of pressure (CoP). The third model (Section 7) extends the second by the addition of a reaction mass and hip actuation, enabling the human-like use of rapid trunk (Horak and Nashner 1986; van der Burg et al. 2005) or arm motions (Roos et al. 2008; Pijnappels et al. 2010).

5. 3D-LIPM with point foot

The 3D-LIPM, described by Kajita and Tanie (1991); Kajita et al. (2001) and depicted in Figure 3, comprises a point mass with position $\mathbf{r}$ at the end of a telescoping massless mechanism (representing the leg), which is in contact with the flat ground. The point mass is kept on a horizontal plane by suitable generalized forces in the mechanism.

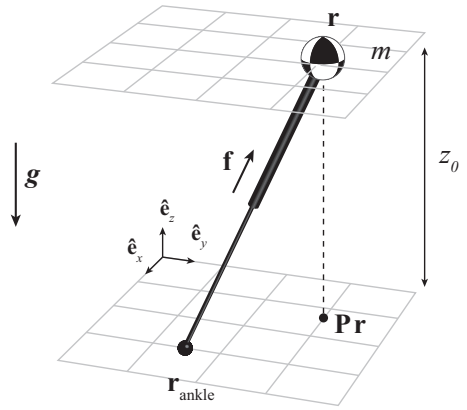

Fig. 3. Schematic representation of the 3D-LIPM with point foot. The model comprises a point foot at position $\mathbf{r}_{\text{ankle}}$, a point mass at position $\mathbf{r}$ with mass m and a massless telescoping leg link with an actuator that exerts a force $\mathbf{f}$ on the point mass that keeps it at constant height z_0. The projection matrix $\mathbf{P}$ projects the point mass location onto the xy-plane. The gravitational acceleration vector is $\mathbf{g}$.

Torques may be exerted at the base of the pendulum. For this first model, however, we set all torques at the base to zero. Hence, the base of the pendulum can be seen as a point foot, with position $\mathbf{r}_{\text{ankle}}$. Foot position changes, which occur when a step is taken, are assumed instantaneous, and have no instantaneous effect on the position and velocity of the point mass.

Following the capturability framework introduced in Section 3, we treat the 3D-LIPM with point foot as a hybrid dynamic system, with dynamics that will be derived in Section 5.1. Its control input is the point foot position. We define a set of allowable values for this control input, described in Section 5.2. The point $\mathbf{r}_{\text{ankle}}$ will be the contact reference point for all models in this paper. Changing the location of the point foot is considered crossing a step surface. The set of failed states for all simple models presented in this paper comprises all states for which $\|\mathbf{r} - \mathbf{r}_{\text{ankle}}\| \to \infty$ as $t \to \infty$, for any allowable control input.

5.1. Equations of motion

The equations of motion for the body mass are

$$m\ddot{\mathbf{r}} = \mathbf{f} + m\mathbf{g} \tag{2}$$

where m is the mass, $\mathbf{r} = \begin{pmatrix} x & y & z \end{pmatrix}^{\mathrm{T}}$ is the position of the center of mass (CoM), expressed in an inertial frame, $\mathbf{f} = \begin{pmatrix} f_x & f_y & f_z \end{pmatrix}^{\mathrm{T}}$ is the actuator force acting on the point mass and $\mathbf{g} = \begin{pmatrix} 0 & 0 & -g \end{pmatrix}^{\mathrm{T}}$ is the gravitational acceleration vector.

A moment balance for the massless link shows that

$$-(\mathbf{r} - \mathbf{r}_{\text{ankle}}) \times \mathbf{f} = \mathbf{0} \tag{3}$$

where $\mathbf{r}_{\text{ankle}} = \begin{pmatrix} x_{\text{ankle}} & y_{\text{ankle}} & 0 \end{pmatrix}^{\mathrm{T}}$ is the location of the ankle.

If $\dot{z} = 0$ initially, the point mass will stay at $z = z_0$ if $\ddot{z} = 0$. Using Equation (2), we find $f_z = mg$. This can be substituted into Equation (3) to find the forces f_x and f_y,

$$f_x = m\omega_0^2(x - x_{\text{ankle}})$$
$$f_y = m\omega_0^2(y - y_{\text{ankle}})$$

where $\omega_0 = \sqrt{\frac{g}{z_0}}$ is the reciprocal of the time constant for the 3D-LIPM.

The equations of motion, (2), can now be rewritten as

$$\ddot{\mathbf{r}} = \omega_0^2(\mathbf{Pr} - \mathbf{r}_{\text{ankle}}) \tag{4}$$

where $\mathbf{P} = \left(\begin{smallmatrix} 1 & 0 & 0 \\ 0 & 1 & 0 \\ 0 & 0 & 0 \end{smallmatrix}\right)$ projects $\mathbf{r}$ onto the xy-plane.

Note that the equations of motion are linear. This linearity is what makes the model valuable as an analysis and design tool, as it allows us to make closed-form predictions. In addition, the equations are decoupled and represent the same dynamics in the x- and y-directions. Each of the first two rows of Equation (4) describes a separate 2D-LIPM with point foot. Therefore, results obtained for the 2D model can readily be extended to the 3D model.

5.2. Allowable control inputs

We introduce two constraints on the stepping capabilities of the model. First, we introduce an upper limit on step length, i.e. the distance between subsequent ankle locations. This maximum step length is denoted $l_{\max}$ and is assumed to be constant; it does not depend on the CoM location $\mathbf{r}$. Second, we introduce a lower limit to the time between steps (ankle location changes), Δt_s, which models swing leg dynamics.

5.3. Dimensional analysis

We perform a dimensional analysis to reduce the number of variables involved and to simplify subsequent derivations. Let us define dimensionless point mass position $\mathbf{r}'$, ankle (point foot) position $\mathbf{r}'_{\text{ankle}}$ and time t' as[1]

$$\mathbf{r}' = \frac{\mathbf{r}}{z_0}, \quad \mathbf{r}'_{\text{ankle}} = \frac{\mathbf{r}_{\text{ankle}}}{z_0}, \quad t' = \omega_0 t.$$

Throughout this paper, the dimensionless counterparts of all positions and lengths will be obtained by dividing by z_0, and times and time intervals will be nondimensionalized by multiplying by ω_0.

The dimensionless point mass position can be differentiated with respect to dimensionless time to obtain dimensionless velocity $\dot{\mathbf{r}}'$ and acceleration $\ddot{\mathbf{r}}'$:

$$\dot{\mathbf{r}}' = \frac{d}{dt'}\mathbf{r}' = \frac{\dot{\mathbf{r}}}{\omega_0 z_0},$$
$$\ddot{\mathbf{r}}' = \frac{d}{dt'}\dot{\mathbf{r}}' = \frac{\ddot{\mathbf{r}}}{\omega_0^2 z_0} = \frac{\ddot{\mathbf{r}}}{g}.$$

Using these dimensionless quantities, the equations of motion, (4), become

$$\ddot{\mathbf{r}}' = \mathbf{P}\mathbf{r}' - \mathbf{r}'_{\text{ankle}}. \tag{5}$$

Further derivations will be simplified by the absence of ω_0 in this equation, as compared with (4).

5.4. Instantaneous capture point

As a first step toward examining N-step capturability, we now introduce the *instantaneous capture point*. For the 3D-LIPM with point foot, it is the point on the ground that enables the system to come to a stop if it were to instantaneously place and maintain its point foot there. Although its definition is motivated by the current model, it will also be useful in the analysis of the other models presented in this part, and we consider it an important quantity to monitor even for more complex, physical, legged systems.

Note that the instantaneous capture point is not necessarily a capture point. According to the definitions given in Section 3, capture points must be reachable, considering the dynamics and actuation limits, while the instantaneous capture point does not take into account the step time or step length constraints as defined in Section 5.2.

The location of the instantaneous capture point can be computed from energy considerations. For a given constant foot position, we can interpret the first two rows of Equation (5) as the descriptions of two decoupled mass–spring systems, each with unit mass and negative unit stiffness. Dimensionless orbital energies (Kajita and Tanie 1991; Kajita et al. 2001), $E'_{\text{LIP},x}$ and $E'_{\text{LIP},y}$, are then defined as the Hamiltonians of these systems:

$$E'_{\text{LIP},x} = \frac{1}{2}\dot{x}'^2 - \frac{1}{2}(x' - x'_{\text{ankle}})^2 \tag{6a}$$

$$E'_{\text{LIP},y} = \frac{1}{2}\dot{y}'^2 - \frac{1}{2}(y' - y'_{\text{ankle}})^2 . \tag{6b}$$

Since Hamiltonians are conserved quantities, so are the orbital energies.

The orbital energy for a direction determines the behavior of the 3D-LIPM in that direction when the CoM is moving toward the foot. Considering the x'-direction for example, three cases of interest arise:

1. $E'_{\text{LIP},x} > 0$. The orbital energy is sufficient to let x' reach x'_{ankle}, after which x' continues to accelerate away from x'_{ankle}.
2. $E'_{\text{LIP},x} < 0$. x' reverses direction before x' reaches x'_{ankle}.
3. $E'_{\text{LIP},x} = 0$. x' comes to a rest exactly at x'_{ankle}.

We can solve for a foot location that results in either desired orbital energies or, equivalently, a desired velocity vector at a given value of $\mathbf{r}'$ (Kajita and Tanie 1991; Kajita et al. 2001). To determine the instantaneous capture point, we are interested in the foot placement required to obtain zero orbital energy in each direction. Solving Equation (6) for $\mathbf{r}'_{\text{ankle}}$ and choosing the solution for which the point mass moves toward the point foot shows that the dimensionless version of the instantaneous capture point (Pratt and Tedrake 2006) is

$$\mathbf{r}'_{\text{ic}} = \mathbf{P}\mathbf{r}' + \dot{\mathbf{r}}' \tag{7}$$

or, in terms of the original physical quantities:

$$\mathbf{r}_{\text{ic}} = \mathbf{P}\mathbf{r} + \frac{\dot{\mathbf{r}}}{\omega_0}. \tag{8}$$

This quantity was independently described by (Hof et al. 2005, 2007; Hof 2008) and named the extrapolated CoM. It was shown to have significant ties to balancing and walking in human test subjects.

5.5. Instantaneous capture point dynamics

If the point foot is not instantaneously placed at the instantaneous capture point, the instantaneous capture point will move. We now analyze this motion. The results of this analysis are depicted graphically in Figure 4. The dynamics that describe the motion of the instantaneous capture point on the ground can be derived by reformulating the dimensionless equations of motion in state space form. The state space model is based on the x'-dynamics only (i.e. the first row of Equation (5), a 2D-LIPM), but the derivations can readily be extended to both directions, as noted in Section 5.1. The first row of Equation (5) is rewritten in state space form as

$$\begin{pmatrix} \dot{x}' \\ \ddot{x}' \end{pmatrix} = \underbrace{\begin{pmatrix} 0 & 1 \\ 1 & 0 \end{pmatrix}}_{\mathbf{A}} \begin{pmatrix} x' \\ \dot{x}' \end{pmatrix} + \underbrace{\begin{pmatrix} 0 \\ -1 \end{pmatrix}}_{\mathbf{B}} x'_{\text{ankle}}. \tag{9}$$

The state matrix $\mathbf{A}$ has eigenvalues $\lambda_{1,2} = \pm 1$ and corresponding eigenvectors

$$\mathbf{V} = \begin{pmatrix} \mathbf{v}_1 & \mathbf{v}_2 \end{pmatrix} = \frac{1}{2}\begin{pmatrix} 1 & 1 \\ 1 & -1 \end{pmatrix}.$$

The eigendata show that there is a saddle point with one stable and one unstable eigenvector. The state matrix can be diagonalized using the similarity transformation $\mathbf{T} = \mathbf{V}^{-1}$, which results in the new state vector

$$\begin{pmatrix} x'_1 \\ x'_2 \end{pmatrix} = \underbrace{\begin{pmatrix} 1 & 1 \\ 1 & -1 \end{pmatrix}}_{\mathbf{T}} \begin{pmatrix} x' \\ \dot{x}' \end{pmatrix}. \tag{10}$$

The new state x'_1 is identical to the instantaneous capture point x'_{ic}, and x'_2 is the point reflection of the instantaneous capture point across the projection of the point mass onto the ground. Note that this change of coordinates was also used by Takenaka et al. (2009). The diagonalized state space model is

$$\begin{pmatrix} \dot{x}'_1 \\ \dot{x}'_2 \end{pmatrix} = \underbrace{\begin{pmatrix} 1 & 0 \\ 0 & -1 \end{pmatrix}}_{\mathbf{TAT}^{-1}} \begin{pmatrix} x'_1 \\ x'_2 \end{pmatrix} + \underbrace{\begin{pmatrix} -1 \\ 1 \end{pmatrix}}_{\mathbf{TB}} x'_{\text{ankle}}. \tag{11}$$

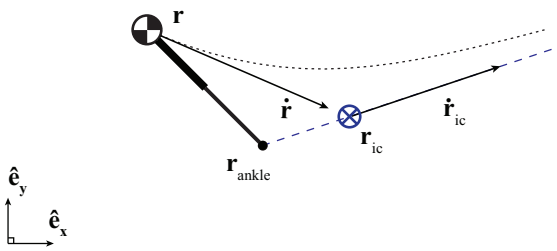

Fig. 4. Top view of the 3D-LIPM with point foot for a given initial state at time t. By adding the CoM velocity vector $\dot{\mathbf{r}}$ (divided by ω_0, see Equation (8)) to the projected CoM position $\mathbf{Pr}$, we find the instantaneous capture point location $\mathbf{r}_{\text{ic}}$. The future trajectories of the point mass and the instantaneous capture point are along the dotted lines for a constant foot location $\mathbf{r}_{\text{ankle}}$. For this figure, $\mathbf{Pr} = [-0.4, 0.4, 0]$, $\dot{\mathbf{r}} = [0.7, -0.3, 0]$, $\mathbf{r}_{\text{ankle}} = [0, 0, 0]$, and model parameters z_0, m, and g are all set to unit magnitude.

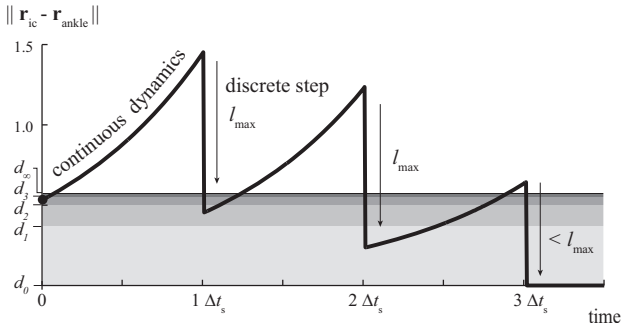

Fig. 5. N-step capturability for the 3D-LIPM with point foot, characterized using the values of d_N (shown for $N \in \{0 \ldots 3, \infty\}$). The quantity d_N is the maximum distance between the instantaneous capture point and the ankle, evaluated at step time, for which the model is N-step capturable. An example initial state is shown, which is 3-step capturable. Note that this state is different from the state depicted in Figure 4. Because the initial state is not 1-step capturable, the distance between the ankle and instantaneous capture point at Δt_{s} is larger than $l_{\max}$. A first step of length $l_{\max}$ towards the instantaneous capture point results in a discrete jump in the distance between the instantaneous capture point and the ankle. A second step is required to make the state 1-step capturable, and a third step is required to reach a captured state. Note that the d_N levels only describe capturability just after a step has been taken: capturability is not in any way reduced during the continuous evolution of the dynamics. For this figure, Δt_{s} and $l_{\max}$ are set to unit magnitude.

The diagonal state matrix TAT^{-1} shows that the model's instantaneous capture point dynamics are first order. State $x'_1 = x'_{\text{ic}}$ corresponds to the unstable eigenvalue $+1$ and is thus of primary interest in stabilizing the system.

These derivations can be repeated for the y'-direction, so that the first row of Equation (11) can be extended to

$$\dot{\mathbf{r}}'_{\text{ic}} = \mathbf{r}'_{\text{ic}} - \mathbf{r}'_{\text{ankle}}. \tag{12}$$

This derivation proves the following theorem:

Theorem 1. *For the 3D-LIPM with point foot, the instantaneous capture point moves on the line through the point foot and itself, away from the point foot, at a velocity proportional to its distance from the point foot.*

As the instantaneous capture point moves away from the foot, its velocity increases exponentially. Figure 4 shows the motion of both the instantaneous capture point and the point mass when the point foot is kept fixed. Note that the projection of the point mass onto the xy-plane describes a hyperbolic curve, as shown by Kajita et al. (2001).

An explicit formulation of the instantaneous capture point trajectory for a fixed foot position is found by solving Equation (12):

$$\mathbf{r}'_{\text{ic}}(\Delta t') = [\mathbf{r}'_{\text{ic}}(0) - \mathbf{r}'_{\text{ankle}}]e^{\Delta t'} + \mathbf{r}'_{\text{ankle}}. \tag{13}$$

This equation will prove useful, both in determining whether a state is N-step capturable and in computing N-step capture regions.

5.6. Capturability

The instantaneous capture point is now used to determine N-step capturability for the 3D-LIPM with point foot. Although computing complete N-step viable-capture basins is possible for this model, we choose to only examine N-step capturability for a part of state space that we consider interesting. The reasons for this choice are brevity and clarity of presentation and because only those parts of the state space need to be considered to compute the N-step capture regions and related capturability measures. For the current model in particular, we will only consider those states for which the model has just taken a step. Denoting the time at which the previous step has been taken $t'_{\text{s,prev}}$, we set $t' = t'_{\text{s,prev}} = 0$.

For the 3D-LIPM with point foot, N-step capturability for these states can be fully described in terms of the initial distance between the contact reference point and the instantaneous capture point, $\left\|\mathbf{r}'_{\text{ic}}(0) - \mathbf{r}'_{\text{ankle}}\right\|$. The maximum distance for which the state is still N-step capturable will be denoted d'_N. Figure 5 shows an evolution that captures the model in the minimum number of steps and the values of d'_N for five values of N. We now proceed to determine these d'_N, first for $N = 0$ and then for the general case.

5.6.1. 0-step capturability The requirement for 0-step capturability follows directly from the definition of the instantaneous capture point, which shows that the model is 0-step capturable if and only if the instantaneous capture point coincides with the point foot location. The requirement for 0-step capturability is thus $\left\|\mathbf{r}'_{\text{ic}}(0) - \mathbf{r}'_{\text{ankle}}\right\| \leq d'_0$, with $d'_0 = 0$ for this model. If this requirement is not met, then $\|\mathbf{r} - \mathbf{r}_{\text{ankle}}\| \to \infty$ as $t \to \infty$ for any evolution that contains no steps.

5.6.2. N-step capturability For higher N, N-step capturability requires being able to reach an $(N-1)$-step capturable state using an evolution that contains only a single step. This is possible if and only if the distance between the foot and the instantaneous capture point, evaluated at the earliest possible step time, Δt_s, is such that there exists a step of allowable length that makes the model $(N-1)$-step capturable:

$$\left\| \mathbf{r}'_{\text{ic}}(\Delta t'_s) - \mathbf{r}'_{\text{ankle}} \right\| \leq d'_{N-1} + l'_{\max}. \tag{14}$$

Using Equation (13), this can be rewritten as

$$\left\| \mathbf{r}'_{\text{ic}}(0) - \mathbf{r}'_{\text{ankle}} \right\| \leq (d'_{N-1} + l'_{\max})\, e^{-\Delta t'_s} = d'_N \tag{15}$$

which leads to a recursive expression for d'_N:

$$d'_N = (d'_{N-1} + l'_{\max})\, e^{-\Delta t'_s}, \quad d'_0 = 0. \tag{16}$$

The maximum distance for N-step capturability, d'_N, follows a converging geometric series, since

$$d'_{N+1} - d'_N = (d'_N - d'_{N-1})\, e^{-\Delta t'_s}, \quad \forall N \geq 1.$$

The ratio of the geometric series, $\exp(-\Delta t'_s) = \exp(-\sqrt{g/z_0}\Delta t_s)$, can be interpreted as a measure of the dynamic mobility of the legged system. The ratio is a dimensionless quantity that takes a value in the interval $[0, 1)$ if the minimum step time is strictly positive. Hence, the series d'_N converges. Moreover, note that being allowed to take more steps to come to a stop suffers from diminishing returns. The nature of the series allows the requirement for ∞-step capturability to be computed in closed form:

$$d'_\infty = d'_0 + \sum_{N=0}^{\infty} \left[d'_{N+1} - d'_N \right] \tag{17a}$$

$$= l'_{\max} \frac{e^{-\Delta t'_s}}{1 - e^{-\Delta t'_s}} \tag{17b}$$

since $d'_0 = 0$ for the 3D-LIPM with point foot.

5.7. Capture regions

The N-step capture regions for the 3D-LIPM with point foot are shown in Figure 6 for an example state. The values of d'_N obtained in the previous section will be used to determine these N-step capture regions in three steps:

1. determine the instantaneous capture point location at the minimum step time;
2. determine the set of possible instantaneous capture point locations before the first step is taken;
3. construct a series of nested regions around this set of possible instantaneous capture point locations.

5.7.1. Instantaneous capture point location after the earliest possible step time The legged system will come to a stop if it steps to the instantaneous capture point. However, stepping is only possible after the minimum step time has passed. Hence, we first determine where the (future) instantaneous capture point will be at the first possible time at which a step can be taken. This point is readily found by substituting $\Delta t' = \Delta t'_s$ into Equation (13).

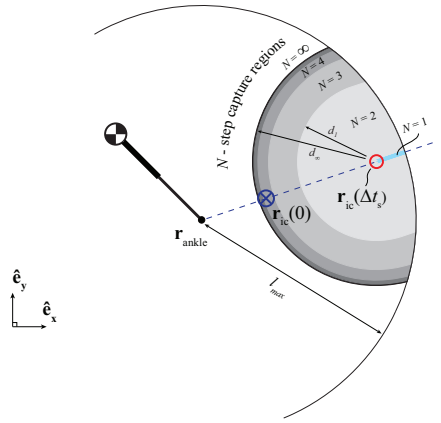

Fig. 6. Top view of the 3D-LIPM with point foot and N-step capture regions, for the same state as shown in Figure 4. In addition to the information in Figure 4, this figure gives a schematic representation of the N-step capture regions for $N \in \{1 \ldots 4, \infty\}$. Before the first step, the instantaneous capture point $\mathbf{r}_{\text{ic}}$ will move away from the point foot, $\mathbf{r}_{\text{ankle}}$, on the dashed line. The set of possible future instantaneous capture point locations for which the minimum step time has passed is the ray starting at $\mathbf{r}_{\text{ic}}(\Delta t_s)$ and pointing along the dashed line, away from the point foot. N-step capture regions are then found as the sets of points within a distance of d_{N-1} to the ray, as long as they lie inside the maximum step length circle. For this figure, model parameters Δt_s and $l_{\max}$ are set to unit magnitude.

5.7.2. Possible instantaneous capture point locations before the first step is taken If a step is not taken at the earliest possible time, the instantaneous capture point will just keep moving farther away from the point foot, as shown by Theorem 1. Therefore, the set of possible future instantaneous capture point locations at $t' \geq \Delta t'_s$ is a ray starting at $\mathbf{r}'_{\text{ic}}(\Delta t'_s)$ which points away from $\mathbf{r}'_{\text{ankle}}$.

5.7.3. Nested regions N-step capture regions for $N \in [1, \infty]$ can be found using this ray and the expression for d'_N in (16). After taking a single step to an N-step capture point, the legged system's state should be $(N-1)$-step capturable. Step locations that put the legged system in such a state are readily found using (16): all points within a distance of d'_{N-1} to a possible instantaneous capture point at $t' \geq \Delta t'_s$ are N-step capture points, provided that the legged system can reach those points given the maximum step length constraint.[2] This results in the nested regions depicted in Figure 6.

Note that finding the 1-step capture region is especially simple. Since $d'_0 = 0$, the step of finding points with distance d'_{N-1} to the ray simply results in the ray itself. The 1-step capture region is then the part of the ray that is inside the maximum step length circle.

6. 3D-LIPM with finite-sized foot

In this section, we extend the 3D-LIPM with point foot by making the foot size finite. The finite-sized foot articulates with the leg at a 2-DoF ankle joint, and is assumed massless. At the ankle, torques may be applied in the pitch and roll directions. However, the torques are limited in such a way that the foot does not start to rotate with respect to the ground. The foot orientation (about the z-axis, i.e. the yaw direction) may be chosen arbitrarily when a step is taken. The model is shown in Figure 7.

6.1. Equations of motion

Only slight modifications to the derivation of the equations of motion for the 3D-LIPM are necessary. Equation (2) also applies to this model. Adding controllable ankle torques $\tau_{\text{ankle},x}$ and $\tau_{\text{ankle},y}$ and a reaction torque $\tau_{\text{ankle},z}$ changes the moment balance of the massless leg link, (3), to

$$-(\mathbf{r} - \mathbf{r}_{\text{ankle}}) \times \mathbf{f} + \boldsymbol{\tau}_{\text{ankle}} = \mathbf{0} \tag{18}$$

where $\boldsymbol{\tau}_{\text{ankle}} = \begin{pmatrix}\tau_{\text{ankle},x} & \tau_{\text{ankle},y} & \tau_{\text{ankle},z}\end{pmatrix}^{\mathrm{T}}$ is the ankle torque and $\mathbf{r}_{\text{ankle}}$ is now the projection of the ankle joint onto the ground.

As before, $f_z = mg$ due to the model constraint $\ddot{z} = 0$, and we find the actuator forces f_x, f_y and the reaction torque $\tau_{\text{ankle},z}$ from Equation (18):

$$\begin{aligned} f_x &= m\omega_0^2(x - x_{\text{ankle}}) + \frac{\tau_{\text{ankle},y}}{z_0} \\ f_y &= m\omega_0^2(y - y_{\text{ankle}}) - \frac{\tau_{\text{ankle},x}}{z_0} \\ \tau_{\text{ankle},z} &= -\frac{\tau_{\text{ankle},x}}{z_0}(x - x_{\text{ankle}}) \\ &\quad -\frac{\tau_{\text{ankle},y}}{z_0}(y - y_{\text{ankle}}). \end{aligned}$$

The equations of motion can then be derived by substituting this into (2), resulting in

$$\ddot{\mathbf{r}} = \omega_0^2(\mathbf{Pr} - \mathbf{r}_{\text{CoP}}) \tag{19}$$

where $\mathbf{r}_{\text{CoP}}$ is the location of the CoP, given by

$$\begin{aligned} \mathbf{r}_{\text{CoP}} &= \mathbf{r}_{\text{ankle}} + \Delta\mathbf{r}_{\text{CoP}}, \\ \Delta\mathbf{r}_{\text{CoP}} &= -\frac{1}{mg}\begin{pmatrix}\tau_{\text{ankle},y} \\ -\tau_{\text{ankle},x} \\ 0\end{pmatrix} = -\frac{\boldsymbol{\tau}_{\text{ankle}} \times \hat{\mathbf{e}}_z}{mg}. \end{aligned}$$

The fact that this is the CoP for this model follows readily from a moment balance for the foot, considering that the ankle torques are such that the foot does not rotate with respect to the ground, by the model definition.

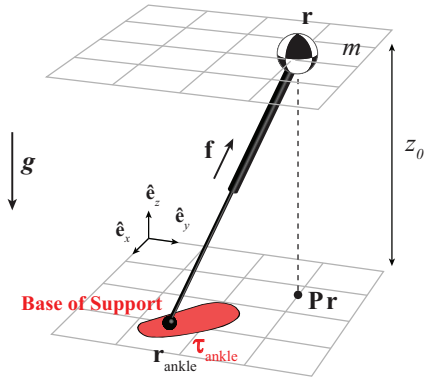

Fig. 7. The 3D-LIPM with finite-sized foot, obtained by extending the 3D-LIPM with point foot (Figure 3) by a finite-sized foot and the ability to apply ankle torques $\boldsymbol{\tau}_{\text{ankle}}$.

Comparing (19) with (4) clearly shows that the dynamics are essentially unchanged. The only difference is that it is now possible to displace the CoP without taking a step. Hence, the results of Section 5.5 are still valid if $\mathbf{r}_{\text{ankle}}$ is replaced by $\mathbf{r}_{\text{CoP}}$.

The dynamics of our 3D-LIPM with finite-sized foot are the same as those of the original 3D-LIPM by Kajita et al. (2001), where the virtual inputs are interpreted as components of an ankle torque vector, expressed in a ground-fixed frame.

6.2. Allowable control inputs

The step length and step time limits as defined for the 3D-LIPM with point foot in Section 5.2 also apply to the 3D-LIPM with finite-sized foot.[3] We augment these allowable control inputs by specifying limits on the ankle torques. The allowable ankle torques are easiest to describe in terms of their resulting CoP location. To fulfill the requirement that the foot must not rotate about its edge, $\mathbf{r}_{\text{CoP}}$ must be kept inside the base of support.[4]

When a step is taken, the foot orientation may be chosen without restriction.

6.3. Dimensional analysis

In addition to the dimensionless quantities defined for the 3D-LIPM with point foot in Section 5.3, we define dimensionless ankle torque $\boldsymbol{\tau}'_{\text{ankle}}$ as

$$\boldsymbol{\tau}'_{\text{ankle}} = \frac{\boldsymbol{\tau}_{\text{ankle}}}{m\omega_0^2 z_0^2}.$$

The dimensionless counterpart of the CoP is then

$$\mathbf{r}'_{\text{CoP}} = \frac{\mathbf{r}_{\text{CoP}}}{z_0} = \mathbf{r}'_{\text{ankle}} - \boldsymbol{\tau}'_{\text{ankle}} \times \hat{\mathbf{e}}_z$$

and the equations of motion reduce to

$$\ddot{\mathbf{r}}' = \mathbf{Pr}' - \mathbf{r}'_{\text{CoP}}. \tag{20}$$

Replacing $\mathbf{r}'_{\text{ankle}}$ by $\mathbf{r}'_{\text{CoP}}$, Equation (12) becomes

$$\dot{\mathbf{r}}'_{\text{ic}} = \mathbf{r}'_{\text{ic}} - \mathbf{r}'_{\text{CoP}} \tag{21}$$

and for a constant CoP, Equation (13) becomes

$$\mathbf{r}'_{\text{ic}}(\Delta t') = [\mathbf{r}'_{\text{ic}}(0) - \mathbf{r}'_{\text{CoP}}]e^{\Delta t'} + \mathbf{r}'_{\text{CoP}}. \tag{22}$$

6.4. Equivalent constant CoP

To find the capture region for this model, the effect of a time-varying CoP must be investigated.

Suppose a time-varying CoP causes the instantaneous capture point to move from an initial position to a final position in a certain time interval. The equivalent constant CoP is the point where the CoP could have been held constant, while it would still move the instantaneous capture point from the initial position to the final position in the same time interval.[5]

We can use Equation (22) to compute the equivalent constant CoP as

$$\mathbf{r}'_{\text{CoP,eq}} = \frac{\mathbf{r}'_{\text{ic}}(\Delta t') - \mathbf{r}'_{\text{ic}}(0)\, e^{\Delta t'}}{1 - e^{\Delta t'}}. \tag{23}$$

Let us now examine the equivalent constant CoP for a piecewise constant CoP trajectory. Suppose the CoP is initially located at $\mathbf{r}'_{\text{CoP},0}$, and is kept there for $\Delta t'_0$. Subsequently, it is changed to $\mathbf{r}'_{\text{CoP},1}$ and kept there for $\Delta t'_1$. The final instantaneous capture point position is found by applying Equation (22) twice:

$$\begin{aligned} \mathbf{r}'_{\text{ic}}(\Delta t'_0) &= [\mathbf{r}'_{\text{ic}}(0) - \mathbf{r}'_{\text{CoP},0}]e^{\Delta t'_0} + \mathbf{r}'_{\text{CoP},0}, \\ \mathbf{r}'_{\text{ic}}(\Delta t'_0 + \Delta t'_1) &= [\mathbf{r}'_{\text{ic}}(\Delta t'_0) - \mathbf{r}'_{\text{CoP},1}]e^{\Delta t'_1} + \mathbf{r}'_{\text{CoP},1}. \end{aligned} \tag{24}$$

Solving Equations (23) and (24) for $\mathbf{r}'_{\text{CoP,eq}}$ (with $\Delta t' = \Delta t'_0 + \Delta t'_1$), we find

$$\mathbf{r}'_{\text{CoP,eq}} = (1 - w')\,\mathbf{r}'_{\text{CoP},0} + w'\mathbf{r}'_{\text{CoP},1} \tag{25}$$

where

$$w' = \frac{e^{\Delta t'_1} - 1}{e^{\Delta t'_0 + \Delta t'_1} - 1}.$$

The dimensionless scalar w' lies in the interval $[0, 1]$ because both $\Delta t'_0$ and $\Delta t'_1$ are non-negative. The equivalent constant CoP is thus a weighted average of the two individual CoPs, where the weighting factors depend only on the time intervals. This statement can be generalized to any number of CoP changes and, in the limit, even to continuously varying CoPs, thus proving the following theorem.

Theorem 2. *For the 3D-LIPM with finite-sized foot, the equivalent constant CoP is a weighted average of the CoP as a function of time.*

The time-varying CoP must always be inside the base of support, which is a convex set. By definition, a weighted average of elements of a convex set must also be in the convex set. Therefore, we have the following result.

Corollary 1. *If the base of support of the 3D-LIPM with finite-sized foot is constant, then the equivalent constant CoP for any realizable instantaneous capture point trajectory lies within the base of support.*

Theorem 2 and Corollary 1 greatly simplify the analysis of capturability and capture regions, since only constant CoP positions within the base of support have to be considered in our subsequent derivations.

Equation (25) reveals some interesting properties of computing the equivalent constant CoP for a piecewise constant CoP trajectory:

- distributivity over addition: adding a constant offset to the individual CoP locations results in an equivalent constant CoP that is offset by the same amount;
- associativity: when computing the equivalent constant CoP for a sequence of three individual CoP locations, the order of evaluation of the composition does not matter;
- non-commutativity: when computing an equivalent constant CoP for a sequence of individual CoP locations, the order of the sequence being composed does matter.

6.5. Capturability

The instantaneous capture point and equivalent constant CoP concepts are now used to determine capturability for the 3D-LIPM with finite-sized foot.

6.5.1. 0-step capturability We first analyze 0-step capturability. We can replace the point foot position by the CoP in Theorem 1 because the model dynamics are equivalent if the ankle position is replaced by CoP. Hence, the instantaneous capture point diverges away from the CoP. Since the base of support is a convex set and cannot change if no step is taken, a corollary of that theorem is as follows.

Corollary 2. *Once the instantaneous capture point of the 3D-LIPM with finite-sized foot is outside the base of support, it is impossible to move it back inside without taking a step.*

Since a captured state can only be reached when the CoP can be made to coincide with the instantaneous capture point, Corollary 2 shows that the 3D-LIPM with finite-sized foot is 0-step capturable if and only if the instantaneous capture point is inside the base of support.

6.5.2. N-step capturability For higher N, capturability is analyzed in much the same way as for the 3D-LIPM with point foot. For the same reasons as mentioned in Section 5.6, we will not compute complete N-step viable-capture basins. For this model we restrict the analysis to states at which a step has just been taken and for which the foot is optimally oriented, in the sense that the distance between the border of the base of support and the instantaneous capture point is minimized, given a fixed ankle location.[6] For

these states, capturability can again be expressed in terms of the distance $\|\mathbf{r}'_{\text{ic}}(0) - \mathbf{r}'_{\text{ankle}}\|$.

The strategy that brings the model to a halt in as few steps as possible comprises stepping as soon as possible in the direction of the instantaneous capture point and always maintaining the CoP as close to the instantaneous capture point as possible.

The CoP should be placed at the point on the edge of the base of support that is closest to the instantaneous capture point. Owing to the assumption of optimal orientation, this point also has the greatest distance to the ankle. This greatest distance will be denoted by $r_{\max}$ and is normalized as $r'_{\max} = r_{\max}/z_0$. The requirement for 0-step capturability thus becomes

$$\|\mathbf{r}'_{\text{ic}}(0) - \mathbf{r}'_{\text{ankle}}\| \leq r'_{\max} = d'_0.$$

Similar to Section 5.6, we can now start at Equation (14) and arrive at formulas for d'_N and d'_∞:

$$d'_N = (l'_{\max} - r'_{\max} + d'_{N-1})\, e^{-\Delta t'_{\text{s}}} + r'_{\max}, \quad N \geq 1 \tag{26a}$$

$$d'_\infty = l'_{\max} \frac{e^{-\Delta t'_{\text{s}}}}{1 - e^{-\Delta t'_{\text{s}}}} + r'_{\max}. \tag{26b}$$

It is seen that the difference between d'_∞ for the model with point foot and d'_∞ for the model with finite-sized foot is simply the normalized maximum distance between the contact reference point and the edge of the foot, $r'_{\max}$.

6.6. Capture regions

The N-step capture regions for the 3D-LIPM with finite-sized foot are shown in Figure 8. The analysis follows the same steps as in Section 5.7.

6.6.1. Possible instantaneous capture point locations at earliest possible step time Owing to the possibility of placing the CoP at any location in the base of support, there is now more than one location where the instantaneous capture point can be at the first time that a step can be taken, i.e. at $\Delta t'_{\text{s}}$. Theorem 2 and Corollary 1 reveal that only constant CoP positions within the base of support need to be considered in this analysis. To find the set of possible instantaneous capture point locations at $\Delta t'_{\text{s}}$, we apply Equation (22) and scan through all possible CoP locations in the base of support. Examining Equation (22) shows that this set of possible instantaneous capture point locations is a scaled point reflection of the base of support across the instantaneous capture point, as shown in Figure 8.

6.6.2. Possible instantaneous capture point locations before the first step is taken If a step is not taken at the earliest possible time, the instantaneous capture point will be pushed farther and farther away by the CoP. Since the CoP can only lie within the base of support, the instantaneous capture point can only be pushed in the directions allowed by Theorem 1 (with point foot replaced by CoP), resulting in the wedge-shaped region of possible instantaneous capture point locations shown in Figure 8. Note that this region is bounded by the 'lines of sight' from the instantaneous capture point to the base of support (dashed lines in Figure 8).

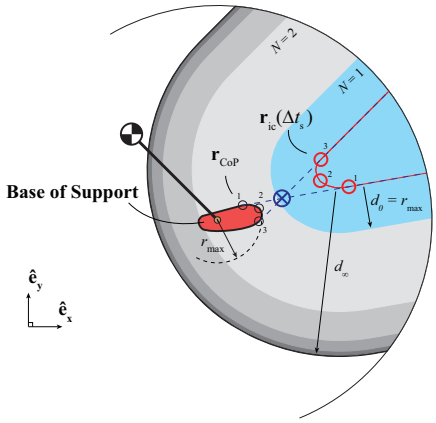

Fig. 8. Top view of the 3D-LIPM with finite-sized foot, showing the N-step capture regions. This figure is an extension of Figure 6: $\mathbf{r}_{\text{ankle}}$, $\mathbf{r}$, and $\dot{\mathbf{r}}$ are identical. We have omitted the labels shown in Figure 6 to avoid cluttering. CoP locations 1 and 3 are just in line of sight of $\mathbf{r}_{\text{ic}}(0)$ and determine to which locations the instantaneous capture point may be directed (dashed lines). CoP location 2 is closest to $\mathbf{r}_{\text{ic}}(0)$ and results in the closest possible location of $\mathbf{r}_{\text{ic}}(\Delta t_{\text{s}})$. The set of all possible instantaneous capture point locations at Δt_{s} is a scaled point reflection of the base of support across the instantaneous capture point (dash-dotted lines), as demonstrated by example CoP locations 1 to 3 and corresponding capture point locations 1 to 3. To obtain the N-step capture regions, the region of possible instantaneous capture point locations before the first step is taken is surrounded by bands of width d'_N, given by Equation (26a). For this figure, $r_{\max} = 0.2$.

6.6.3. Nested regions To find the N-step capture regions, we follow the same procedure as in Section 5.7, that is, we create nested regions around the region of possible instantaneous capture point locations. This time, the greatest allowed distance to the possible instantaneous capture point locations is computed using Equation (26a) instead of Equation (16). This method assumes that the foot orientation will be chosen optimally when the step is taken. Note that for this model, $d'_0 = r'_{\max} > 0$, as opposed to the previous model. Discarding points that are outside the maximum step length circle results in the final N-step capture regions for this model.

7. 3D-LIPM with finite-sized foot and reaction mass

We now extend the 3D-LIPM with finite-sized foot by modeling not just a point 'body' mass at the end of the leg, but

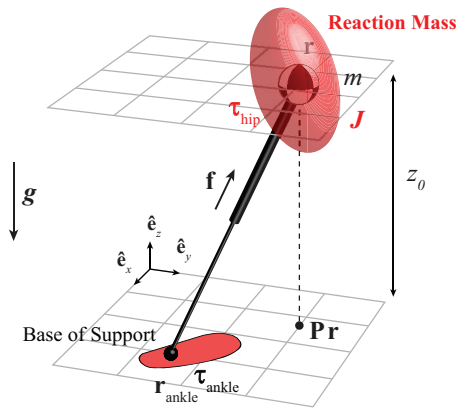

Fig. 9. The 3D-LIPM with finite-sized foot and reaction mass. The 3D-LIPM with finite-sized foot (Figure 7) is extended with a non-zero mass moment of inertia tensor $\mathbf{J}$ and the ability to apply hip torques $\boldsymbol{\tau}_{\text{hip}}$ to obtain the 3D-LIPM with finite-sized foot and reaction mass.

a rigid body possessing a non-zero mass moment of inertia. Actuators in the hip can exert torques on this reaction mass in all directions, enabling lunging motions in 3D. The model, depicted in Figure 9, is a 3D version of the Linear Inverted Pendulum plus Flywheel Model presented by Pratt et al. (2006). It can also be considered as a linear version of the Reaction Mass Pendulum (Lee and Goswami 2007) with a constant mass moment of inertia.

To make the analysis tractable, we specify several constraints. We place limits on the allowable angle of the reaction mass with respect to the vertical axis. At the start of our analysis, we assume that both this angle and the angular velocity of the body are zero. Hip torques can be used to accelerate the reaction mass, but must be followed by decelerating torques to prevent the reaction mass from exceeding its angle limit. Furthermore, we assume that the robot can only lunge once, in only one direction, similar to a human using a single impulsive lunging response in an attempt to regain balance after a severe perturbation. In addition to angle limits, we place limits on the allowable hip torque. The hip torque component around the z-axis is determined by the requirement of no yaw of the reaction mass. This requirement makes the equations of motion linear. For the horizontal torque components, we assume a bang–bang input profile, as used by Stephens (2007a,b). We assume in the analysis that the execution time of the profile is less than the minimum step time and that the CoP is held constant while the torque profile is executed.

7.1. Equations of Motion

The equations of motion for the reaction mass are

$$m\ddot{\mathbf{r}} = \mathbf{f} + m\mathbf{g}, \tag{27a}$$

$$\mathbf{J}\dot{\boldsymbol{\omega}} = \boldsymbol{\tau}_{\text{hip}} - \boldsymbol{\omega}\times(\mathbf{J}\boldsymbol{\omega}), \tag{27b}$$

where $\boldsymbol{\omega} = \begin{pmatrix}\omega_x & \omega_y & \omega_z\end{pmatrix}^{\mathrm{T}}$ is the angular velocity vector of the upper body, expressed in the inertial reference frame, $\boldsymbol{\tau}_{\text{hip}} = \begin{pmatrix}\tau_{\text{hip},x} & \tau_{\text{hip},y} & \tau_{\text{hip},z}\end{pmatrix}^{\mathrm{T}}$ is the hip torque vector, $\mathbf{J}$ is the mass moment of inertia in the body-fixed frame, and m, $\mathbf{r}$, $\mathbf{f}$ and $\mathbf{g}$ are as defined in Section 5.1.

Assuming that $\omega_z = 0$, that $\tau_{\text{hip},z}$ is such that $\dot{\omega}_z = 0$, and that $\mathbf{J}$ is diagonal, Equation (27b) can be rewritten as

$$\begin{aligned} J_{xx}\dot{\omega}_x &= \tau_{\text{hip},x} \\ J_{yy}\dot{\omega}_y &= \tau_{\text{hip},y} \\ 0 &= \tau_{\text{hip},z} + (J_{xx} - J_{yy})\,\omega_x\omega_y. \end{aligned}$$

This last equation specifies the hip torque about the z-axis that is required to keep the reaction mass from yawing. Note that no hip torque about the z-axis is required if $J_{xx} = J_{yy}$.

The moment balance for the massless leg link is

$$-(\mathbf{r} - \mathbf{r}_{\text{ankle}}) \times \mathbf{f} - \boldsymbol{\tau}_{\text{hip}} + \boldsymbol{\tau}_{\text{ankle}} = \mathbf{0}. \tag{28}$$

Keeping the mass at $z = z_0$ means that $f_z = mg$, as before. This fact and Equation (28) can be used to find the reaction forces f_x and f_y, and the ankle torque $\tau_{\text{ankle},z}$:

$$\begin{aligned} f_x &= m\omega_0^2(x - x_{\text{CoP}}) - \frac{\tau_{\text{hip},y}}{z_0}, \\ f_y &= m\omega_0^2(y - y_{\text{CoP}}) + \frac{\tau_{\text{hip},x}}{z_0}, \\ \tau_{\text{ankle},z} &= \frac{\tau_{\text{hip},x} - \tau_{\text{ankle},x}}{z_0}(x - x_{\text{ankle}}) \\ &\quad + \frac{\tau_{\text{hip},y} - \tau_{\text{ankle},y}}{z_0}(y - y_{\text{ankle}}) + \tau_{\text{hip},z}. \end{aligned}$$

We can now rewrite Equation (27) to obtain the equations of motion,

$$\ddot{\mathbf{r}} = \omega_0^2(\mathbf{P}\mathbf{r} - \mathbf{r}_{\text{CMP}}), \tag{29a}$$

$$\dot{\boldsymbol{\omega}} = \mathbf{J}^{-1}\mathbf{P}\boldsymbol{\tau}_{\text{hip}}, \tag{29b}$$

where $\mathbf{r}$, ω_0 and $\mathbf{P}$ are as defined in Section 5.1, and

$$\mathbf{r}_{\text{CMP}} = \mathbf{r}_{\text{CoP}} + \Delta\mathbf{r}_{\text{CMP}}, \tag{30a}$$

$$\Delta\mathbf{r}_{\text{CMP}} = \frac{1}{mg}\begin{pmatrix}\tau_{\text{hip},y} \\ -\tau_{\text{hip},x} \\ 0\end{pmatrix} = \frac{\boldsymbol{\tau}_{\text{hip}} \times \hat{\mathbf{e}}_z}{mg}. \tag{30b}$$

The point $\mathbf{r}_{\text{CMP}}$ is the centroidal moment pivot (CMP) as defined in Popovic et al. (2005). Here we have used the fact that the CoP is equal to the ZMP when the ground is flat and horizontal (Popovic et al. 2005).

The equations of motion are again linear. Note the similarity to the equations of motion for the previous models, which allows us to reuse most results obtained for those models if the CoP is replaced by the CMP.

7.2. Allowable control inputs

The actuation limits of the 3D-LIPM with finite-sized foot are extended to include the hip torque profile. The set

of allowable hip torque profiles is the set of bang–bang torque profiles for which the torque and angle limits are not exceeded at any time. These torque profiles can be written as

$$\mathbf{P}\boldsymbol{\tau}_{\text{hip}} = \tau_{\text{hip}}\hat{\mathbf{e}}_\tau[u(t) - 2u(t-\Delta t_{\text{RM}}) + u(t-2\Delta t_{\text{RM}})], \quad (31)$$

where τ_{hip} is the torque magnitude, $\hat{\mathbf{e}}_\tau$ is the torque direction, $u(\cdot)$ is the Heaviside step function, and Δt_{RM} is the duration of each torque 'bang'. The hip torque magnitude is limited as $\tau_{\text{hip}} \leq \tau_{\text{hip,max}}$.

To comply with model assumptions, the angular velocity of the reaction mass must be zero both before and after the application of the hip torque profile, so both bangs must have equal duration. For a 2D version of the presented model, Stephens (2007b) and Pratt et al. (2006) have shown that this duration has a maximum value

$$\Delta t_{\text{RM,max}} = \sqrt{J\theta_{\max}/\tau_{\text{hip}}} \quad (32)$$

given the scalar mass moment of inertia J, the angle limit $\theta_{\max}$ with respect to vertical, and the hip torque τ_{hip}. The appropriate scalar inertia value for the model presented here can be obtained from the mass moment of inertia tensor and the torque direction as $J = \hat{\mathbf{e}}_\tau^{\mathrm{T}}\mathbf{J}\hat{\mathbf{e}}_\tau$.

7.3. Dimensional analysis

Additional dimensionless quantities are needed to non-dimensionalize the equations of motion. We define the dimensionless mass moment of inertia $\mathbf{J}'$, angular velocity $\boldsymbol{\omega}'$, and hip torque $\boldsymbol{\tau}'_{\text{hip}}$ as

$$\mathbf{J}' = \frac{\mathbf{J}}{mz_0^2}, \quad \boldsymbol{\omega}' = \frac{\mathbf{J}'\boldsymbol{\omega}}{\omega_0}, \quad \boldsymbol{\tau}'_{\text{hip}} = \frac{\boldsymbol{\tau}_{\text{hip}}}{m\omega_0^2 z_0^2}.$$

The dimensionless angular velocity $\boldsymbol{\omega}'$ is differentiated with respect to dimensionless time t' to obtain dimensionless angular acceleration:

$$\dot{\boldsymbol{\omega}}' = \frac{d}{dt'}\boldsymbol{\omega}' = \frac{\mathbf{J}'\dot{\boldsymbol{\omega}}}{\omega_0^2}.$$

The dimensionless version of the CMP is

$$\mathbf{r}'_{\text{CMP}} = \frac{\mathbf{r}_{\text{CMP}}}{z_0} = \mathbf{r}'_{\text{CoP}} + \Delta\mathbf{r}'_{\text{CMP}}, \quad (33a)$$

$$\Delta\mathbf{r}'_{\text{CMP}} = \boldsymbol{\tau}'_{\text{hip}} \times \hat{\mathbf{e}}_z. \quad (33b)$$

These quantities can be used to rewrite the equations of motion, (29), as

$$\ddot{\mathbf{r}}' = \mathbf{P}\mathbf{r}' - \mathbf{r}'_{\text{CMP}}, \quad (34a)$$

$$\dot{\boldsymbol{\omega}}' = \mathbf{P}\boldsymbol{\tau}'_{\text{hip}}. \quad (34b)$$

Replacing $\mathbf{r}'_{\text{CoP}}$ by $\mathbf{r}'_{\text{CMP}}$, (21) becomes

$$\dot{\mathbf{r}}'_{\text{ic}} = \mathbf{r}'_{\text{ic}} - \mathbf{r}'_{\text{CMP}} \quad (35)$$

and for a constant CMP, Equation (22) becomes

$$\mathbf{r}'_{\text{ic}}(\Delta t') = [\mathbf{r}'_{\text{ic}}(0) - \mathbf{r}'_{\text{CMP}}]e^{\Delta t'} + \mathbf{r}'_{\text{CMP}}. \quad (36)$$

7.4. Effect of the hip torque profile

To analyze capturability for this model, we first examine how the hip torque profile influences the instantaneous capture point motion.

Since the CoM dynamics of the current model, (34a), are the same as those of the previous model, (19), with the CoP replaced by the CMP, we can reuse the equivalent constant CoP concept from Section 6.4. During the application of the hip torque profile, the CMP will first be held constant at $\mathbf{r}'_{\text{CoP}} + \tau'_{\text{hip}}\hat{\mathbf{e}}_\tau \times \hat{\mathbf{e}}_z$ for $\Delta t'_{\text{RM}}$, after which it moves to $\mathbf{r}'_{\text{CoP}} - \tau'_{\text{hip}}\hat{\mathbf{e}}_\tau \times \hat{\mathbf{e}}_z$ when the torque direction is reversed, and stays there for another $\Delta t'_{\text{RM}}$. The equivalent constant CMP is found using Equation (25), with $\Delta t'_0 = \Delta t'_1 = \Delta t'_{\text{RM}}$:

$$\mathbf{r}'_{\text{CMP,eq}} = \mathbf{r}'_{\text{CoP}} + (1 - 2w')\,\tau'_{\text{hip}}\hat{\mathbf{e}}_\tau \times \hat{\mathbf{e}}_z. \quad (37)$$

The final location of the instantaneous capture point can then be computed using (36):

$$\mathbf{r}'_{\text{ic}}(2\Delta t'_{\text{RM}}) = [\mathbf{r}'_{\text{ic}}(0) - \mathbf{r}'_{\text{CMP,eq}}]e^{2\Delta t'_{\text{RM}}} + \mathbf{r}'_{\text{CMP,eq}}.$$

Using Equation (37), this can be rewritten as

$$\mathbf{r}'_{\text{ic}}(2\Delta t'_{\text{RM}}) = [\mathbf{r}'_{\text{ic}}(0) - \mathbf{r}'_{\text{CMP}*}]e^{2\Delta t'_{\text{RM}}} + \mathbf{r}'_{\text{CoP}} \quad (38)$$

where

$$\mathbf{r}'_{\text{CMP}*} = \mathbf{r}'_{\text{CoP}} + \Delta\mathbf{r}'_{\text{CMP}*}, \quad (39a)$$

$$\Delta\mathbf{r}'_{\text{CMP}*} = v'\tau'_{\text{hip}}\hat{\mathbf{e}}_\tau \times \hat{\mathbf{e}}_z, \quad (39b)$$

$$v' = (1 - 2w')(1 - e^{-2\Delta t'_{\text{RM}}}) \quad (39c)$$

$$= 1 - 2e^{-\Delta t'_{\text{RM}}} + e^{-2\Delta t'_{\text{RM}}}. \quad (39d)$$

The vector $\Delta\mathbf{r}'_{\text{CMP}*}$ expresses the influence of the hip torque profile on the instantaneous capture point motion. The scalar v' can be shown to monotonically increase from 0 to 1 for $\Delta t'_{\text{RM}} > 0$.

Equation (38) shows that $\|\Delta\mathbf{r}'_{\text{CMP}*}\|$ must be maximized to gain a maximal effect of the hip torque profile on the final instantaneous capture point location. It can be shown that

$$\arg\max \|\Delta\mathbf{r}'_{\text{CMP}*}(\tau'_{\text{hip}})\| = \tau'_{\text{hip,max}}. \quad (40)$$

That is, even though increasing hip torque τ'_{hip} reduces the allowed torque duration $\Delta t'_{\text{RM}}$ according to Equation (32), the linear term in Equation (39b) outweighs the reduced value of v'. The maximum value of $\|\Delta\mathbf{r}'_{\text{CMP}*}\|$ will be denoted $\|\Delta\mathbf{r}'_{\text{CMP}*}\|_{\max}$.

7.5. Capturability

The results from Section 7.4 will now be used to investigate capturability.

7.5.1. 0-step capturability With a reaction mass, the model can be 0-step capturable even if the instantaneous capture point is not initially located inside the base of support. Rather, the requirement for 0-step capturability is that

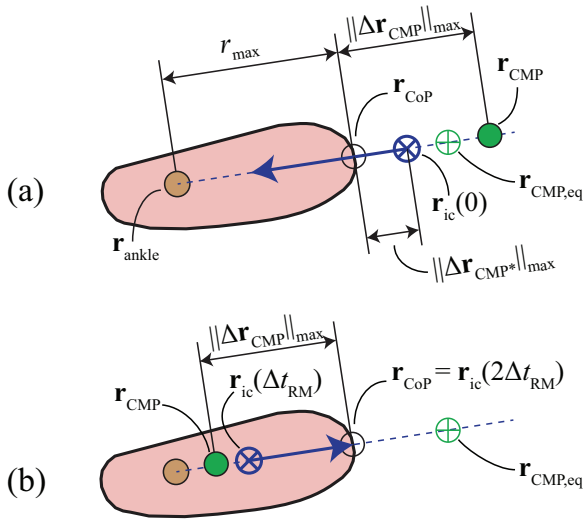

Fig. 10. Instantaneous capture point motion during the hip torque profile, for the boundary case described in Section 7.5.1. (a) $t \in [0, \Delta t_{RM})$: during the first half of the hip torque profile, the CMP maximally pushes the instantaneous capture point inside the base of support. (b) $t \in [\Delta t_{RM}, 2\Delta t_{RM}]$: during the 'payback phase', the CMP must be placed in the opposite direction to stop the spinning motion of the reaction mass. The net effect is that the instantaneous capture point ends up on the boundary of the base of support at $2\Delta t'_{RM}$, exactly at the CoP. Note that the figure shows a special case where the foot is optimally oriented.

the instantaneous capture point should be inside the base of support after the application of the torque profile. To determine which states are 0-step capturable, we examine a boundary case for which the instantaneous capture point can only just be pushed from outside the base of support back to its edge (see Figure 10).

For this boundary case, it is best to place the CoP as close to the initial instantaneous capture point as possible, thus minimizing its rate of divergence. As the instantaneous capture point needs to be pushed back to the boundary of the base of support and the optimal CoP location is the closest point on that boundary, we have $\mathbf{r}'_{ic}(2\Delta t'_{RM}) = \mathbf{r}'_{CoP}$. The hip torque profile should always be applied as soon as possible to be most effective, since waiting longer simply results in an initial instantaneous capture point location that is farther removed from the foot. Using this information together with Equations (39a) and (38), we obtain

$$\begin{aligned} \mathbf{r}'_{CoP} &= [\mathbf{r}'_{ic}(0) - \mathbf{r}'_{CoP} - \Delta \mathbf{r}'_{CMP*}] e^{2\Delta t'_{RM}} + \mathbf{r}'_{CoP} \\ \therefore \left\| \mathbf{r}'_{ic}(0) - \mathbf{r}'_{CoP} \right\|_{max} &= \left\| \Delta \mathbf{r}'_{CMP*} \right\|_{max} \end{aligned}$$

for the boundary case. Since the hip torque may be exerted in any direction and the CoP may be anywhere inside the base of support, the system is 0-step capturable in the general case if and only if the initial distance between the instantaneous capture point and the base of support is smaller than or equal to $\left\| \Delta \mathbf{r}'_{CMP*} \right\|_{max}$.

7.5.2. N-step capturability For N-step capturability, we restrict the analysis to states in which a step has just been taken, the foot is optimally oriented, and the reaction mass starts in the upright position.

For these states, the strategy that brings the model to a stop in as few steps as possible consists of stepping as soon as possible, choosing the CoP location as close as possible to the initial instantaneous capture point and lunging as soon and as hard as possible in the direction of the initial instantaneous capture point.

While this strategy is being executed, $\mathbf{r}'_{ic}$, $\mathbf{r}'_{CoP}$, $\mathbf{r}'_{CMP}$, and $\mathbf{r}'_{ankle}$ are all on the same line due to optimal orientation of the foot (as in Figure 10). The requirement for 0-step capturability can thus be simplified for these states and written in terms of the distance to the contact reference point $\mathbf{r}'_{ankle}$ as

$$\begin{aligned} \left\| \mathbf{r}'_{ic}(0) - \mathbf{r}'_{ankle} \right\| &\leq r'_{max} + \left\| \Delta \mathbf{r}'_{CMP*} \right\|_{max} \\ &= d'_0. \end{aligned} \tag{41}$$

The limit of capturability for $N = 1$ is calculated as follows. At the end of the torque profile, the instantaneous capture point location is determined by Equation (38). The motion of the instantaneous capture point between the end of the torque profile and the minimum swing time is governed by Equation (36). Composing these equations results in the instantaneous capture point location at the minimum step time:

$$\mathbf{r}'_{ic}(\Delta t'_s) - \mathbf{r}'_{CoP} = (\mathbf{r}'_{ic}(0) - \mathbf{r}'_{CMP*}) e^{\Delta t'_s}. \tag{42}$$

Using the definitions of $\mathbf{r}'_{CoP}$ and $\mathbf{r}'_{CMP*}$, the fact that all points involved lie on the same line, and maximizing the influence of the hip torque profile by using $\left\| \Delta \mathbf{r}'_{CMP*} \right\| = \left\| \Delta \mathbf{r}'_{CMP*} \right\|_{max}$, we have

$$\begin{aligned} &\left\| \mathbf{r}'_{ic}(\Delta t'_s) - \mathbf{r}'_{CoP} \right\| = \left\| \mathbf{r}'_{ic}(\Delta t'_s) - \mathbf{r}'_{ankle} \right\| - r'_{max}, \\ &\left\| \mathbf{r}'_{ic}(0) - \mathbf{r}'_{CMP*} \right\| = \\ &\qquad \left\| \mathbf{r}'_{ic}(0) - \mathbf{r}'_{ankle} \right\| - (r'_{max} + \left\| \Delta \mathbf{r}'_{CMP*} \right\|_{max}). \end{aligned}$$

We can use this in combination with (42) to find

$$\begin{aligned} \left\| \mathbf{r}'_{ic}(\Delta t'_s) - \mathbf{r}'_{ankle} \right\| &= \left\| \mathbf{r}'_{ic}(0) - \mathbf{r}'_{ankle} \right\| e^{\Delta t'_s} \\ &\quad - (r'_{max} + \left\| \Delta \mathbf{r}'_{CMP*} \right\|_{max}) e^{\Delta t'_s} + r'_{max}. \end{aligned} \tag{43}$$

Since usage of the reaction mass is no longer available after the first step is taken, the model is essentially reduced to the model presented in Section 6, so the requirement for 1-step capturability is that the instantaneous capture point is located inside the base of support right after the first step is taken. Stepping in the direction of the instantaneous capture point reduces its distance to the ankle by at most l'_{max}, and after the step the instantaneous capture point should be at most r'_{max} away from the ankle to be 0-step capturable. The criterion for 1-step capturability is therefore

$$\left\| \mathbf{r}'_{ic}(\Delta t'_s) - \mathbf{r}'_{ankle} \right\| \leq l'_{max} + r'_{max}.$$

Using Equation (43), this becomes

$$\left\|\mathbf{r}'_{\text{ic}}(0)-\mathbf{r}'_{\text{ankle}}\right\| \leq l'_{\max}e^{-\Delta t'_{\text{s}}}+r'_{\max} + \left\|\Delta\mathbf{r}'_{\text{CMP}*}\right\|_{\max}=d'_1. \quad (44)$$

For both 0-step and 1-step capturability, we see that the margin that is gained by the addition of the reaction mass is $\left\|\Delta\mathbf{r}'_{\text{CMP}*}\right\|_{\max}$, compared with Equation (26a). Recursively applying the above derivations shows that this trend continues for all N, so that

$$d'_N = (l'_{\max}-r'_{\max}+d'_{N-1})\,e^{-\Delta t'_{\text{s}}} + r'_{\max}+\left\|\Delta\mathbf{r}'_{\text{CMP}*}\right\|_{\max}, \quad N\geq 1 \quad (45a)$$

$$d'_\infty = l'_{\max}\frac{e^{-\Delta t'_{\text{s}}}}{1-e^{-\Delta t'_{\text{s}}}}+r'_{\max}+\left\|\Delta\mathbf{r}'_{\text{CMP}*}\right\|_{\max}. \quad (45b)$$

7.6. Capture regions

The N-step capture regions for the 3D-LIPM with finite-sized foot and reaction mass are shown in Figure 11 and are derived as follows.

7.6.1. Possible instantaneous capture point locations at earliest possible step time Similar to the previous models, the first step to finding the capture regions is to find the set of possible future instantaneous capture point locations at time $\Delta t'_{\text{s}}$. The difference that the reaction mass makes is found by rewriting Equation (38) as

$$\mathbf{r}'_{\text{ic}}(\Delta t'_{\text{s}}) = \mathbf{r}'_{\text{ic}}(\Delta t'_{\text{s}})\big|_{\tau'_{\text{hip}}=0} - \Delta\mathbf{r}'_{\text{CMP}*}e^{\Delta t'_{\text{s}}} \quad (46)$$

where $\mathbf{r}'_{\text{ic}}(\Delta t'_{\text{s}})\big|_{\tau'_{\text{hip}}=0}$ is the instantaneous capture point location at $\Delta t'_{\text{s}}$ when no hip torque is applied, that is, when $\Delta\mathbf{r}'_{\text{CMP}*}=0$, for which the model reduces to the model without reaction mass. Taking the hip torque limit into account results in

$$\left\|\mathbf{r}'_{\text{ic}}(\Delta t'_{\text{s}})\big|_{\tau'_{\text{hip}}=0}-\mathbf{r}'_{\text{ic}}(\Delta t'_{\text{s}})\right\| \leq \delta$$

where

$$\delta = \left\|\Delta\mathbf{r}'_{\text{CMP}*}\right\|_{\max}e^{\Delta t'_{\text{s}}}.$$

Therefore, the set of possible instantaneous capture point locations at time $\Delta t'_{\text{s}}$ consists of all points that lie at most δ away from possible instantaneous capture point locations at $\Delta t'_{\text{s}}$ for the model without reaction mass (see Section 6.6.1).

7.6.2. Possible instantaneous capture point locations after the earliest possible step time After the application of the hip torque profile, the CMP will coincide with the CoP, and the instantaneous capture point will move on a line through itself and the CoP. Bounds on reachable instantaneous capture point locations are therefore found exactly as in Section 6.6.2, by constructing lines of sight (shown as the dashed lines in Figure 11) from the base of support to the set of possible instantaneous capture point locations at $\Delta t'_{\text{s}}$.

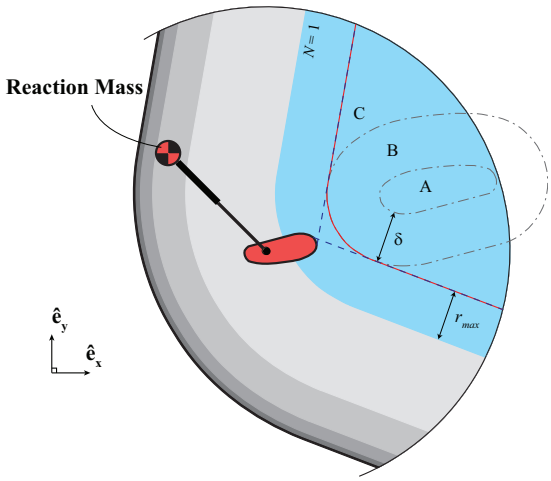

Fig. 11. Top view of the 3D-LIPM with finite-sized foot and reaction mass, with a schematic representation of the N-step capture regions. The figure is an extension of Figure 8: state parameters $\mathbf{r}_{\text{ankle}}$, $\mathbf{r}$ and $\dot{\mathbf{r}}$ are identical. We have omitted labels that were already shown in Figure 8 to avoid cluttering. The geometric construction is as follows. (1) Find region A as described in Figure 8 and find region B by offsetting region A by δ; (2) use the lines of sight from the base of support to find region C; (3) find the capture regions by offsetting region C by the values of d_N from Equation (26a). For this figure, $\tau_{\text{hip,max}}$ is set to 0.5 and $\theta_{\max}=1/8$, which results in a total lunge time ($2\Delta t_{\text{RM,max}}$) of 1.

7.6.3. Nested regions Finally, we can construct capture regions exactly as in Section 6.6.3. After the first step is taken, no further hip torque is applied and the model essentially reduces to the 3D-LIPM with finite-sized foot. We should hence construct nested regions around the set of possible future instantaneous capture point locations using the values of d'_N for the LIPM *without* reaction mass, i.e. those calculated using Equation (26a), not those from Equation (45a). The effect of the reaction mass is already incorporated in the set of possible instantaneous capture point locations at the earliest possible step time.

8. Capturability comparison

For all three models, we determined which states in a subset of state space are N-step capturable, and derived descriptions of the N-step capture regions. The N-step capture regions of Figures 6, 8, and 11 clearly showed that an increase in the number of possible stabilizing mechanisms leads to an increase in capture region size. This result implies that there is more freedom to choose foot placements that keep the model capturable, or we could say that the 'level of capturability' increases.

For a specific state, the area of the N-step capture region can be used as a measure of capturability. We call this the N-step capturability margin. This metric expresses how close a specific state of a system is to not being N-step capturable.

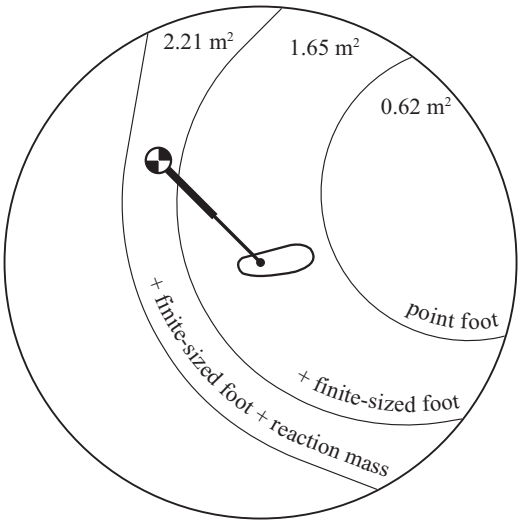

Fig. 12. Superimposed ∞-step capture regions of all three models, as previously presented in Figures 6, 8, and 11. The sizes of the ∞-step capture regions, i.e. the ∞-step capturability margins, are shown.

It also gives an indication of the input deviations and disturbances that are allowed while executing a given evolution. A small size of the ∞-step capture region, for example, indicates that a small disturbance will likely make the legged system fall.

In the previous sections, we graphically depicted the influence of the various model parameters on the ∞-step capture region for a given initial state. Figure 12 combines these results and displays the size of the three ∞-step capture regions. Parameters were set to estimated anthropomorphic values, as presented in Appendix A. For the selected initial state, the addition of a finite-sized foot caused the ∞-step capturability margin to increase by 160%. Another increase of 30% was found for the addition of the reaction mass.

Instead of considering a specific state, we can also consider the capturability of a model in general. The d_∞ capturability level, which was computed for all three models, gives an indication of the overall legged-system stability and allows a comparison. In terms of the original physical quantities, d_∞ for the 3D-LIPM with finite-sized foot and reaction mass is expressed as

$$d_\infty = \underbrace{l_{\max}\frac{e^{-\omega_0 \Delta t_s}}{1-e^{-\omega_0 \Delta t_s}}}_{\text{3D-LIPM, Section 5}} + \underbrace{r_{\max}}_{\text{3D-LIPM,Section 6}} + \underbrace{\frac{\tau_{\text{hip,max}}}{m\omega_0^2 z_0}\left[1-2e^{-\omega_0 \Delta t_{\text{RM,max}}}+e^{-2\omega_0 \Delta t_{\text{RM,max}}}\right]}_{\text{3D-LIPM, Section 7}}. \quad (47)$$

For the model with point foot, $d_\infty = 0.431$ using anthropometric parameters. Adding a finite-sized base of support results in $d_\infty = 0.631$, and an additional reaction mass results in $d_\infty = 0.664$.

9. Discussion

9.1. Simple models

To analyze capturability for the three presented walking models, we made extensive use of the instantaneous capture point, which is determined only by the CoM position and velocity. This gave us a dimensionally reduced description of the dynamics of the three models. We showed how this resulted in relatively simple and comprehensible expressions, and enabled calculation and visualization of capture regions and viable-capture basins.

The three models revealed the relation between the location of the point foot, the CoP and the CMP in the analysis of capturability. Despite time variant inputs, the dynamics of the instantaneous capture point remains easy to predict for all three models: the instantaneous capture point diverges away from the CMP along a straight line at a velocity proportional to the distance to the CMP. The CMP reduces to the CoP if no reaction mass is present or actuated. The CoP reduces to the point foot location if the base of support is infinitesimally small.

The LIPM with point foot suggests that in order to remain capturable, the foot should be placed sufficiently quickly in the direction of the instantaneous capture point. This simple stepping strategy was used to create a variety of stable locomotion patterns in simulation (Pratt and Tedrake 2006; Yin et al. 2007) and was also found to be a good predictor of stable foot placement locations in the analysis of human walking (Townsend 1985; Hof 2008; Millard et al. 2009; Hof et al. 2010).

The analysis for the LIPM with finite-sized foot introduced the equivalent constant CoP, which greatly simplifies the analysis of the presented models. This equivalent constant CoP is a useful analysis tool and can also be applied to robot control, as demonstrated recently (Englsberger et al. 2011).

The LIPM with finite-sized foot and reaction mass showed that lunging as soon as possible in the direction of the instantaneous capture point maximizes the level of capturability. We conjecture that bang–bang control achieves the maximal influence on instantaneous capture point motion if lunging is constrained by angle and torque limits. Note that in general it is not straightforward to relate the effect of the angular momentum generated by the simple reaction mass to the effect generated by all individual links of a complex multibody system (Lee and Goswami 2007; Orin and Goswami 2008). However, this simple model still demonstrates the conceptual contribution of angular momentum to the stability of locomotion.

The influence of each stabilizing mechanism on the capturability of each model was demonstrated by Equation (47). The values of d_∞ obtained for human parameters suggest that, not surprisingly, the ability to perform rapid steps is most important to remain capturable. This suggestion is also expressed by the metric being most sensitive to changes in minimum step time. A variation in

minimum step time can be compensated by another stabilizing mechanism to retain the same level of capturability. However, a 10% increase in step duration already requires a 17% longer step or a 30% longer foot. For humans, selection of the appropriate step speed and length may be a trade-off between the required muscle strength to perform a quick step (Thelen et al. 1997; Smeesters et al. 2001) and the perceived level of stability or safety of the selected step length (Maki and McIlroy 1999; Weerdesteyn et al. 2005; Hsiao-Wecksler and Robinovitch 2007).

The use of the three presented simple models as a representation of legged locomotion has a number of limitations. The models discard many aspects of legged locomotion. Height variations of the CoM during legged locomotion were not considered. Internal forces generated by lunging or swing leg dynamics were discarded. Slippage or losses at the change of support were not considered. The existence of a double support phase in case of walking was also not taken into account. Consequently, using these simple models to approximate the capturability of a real robot will lead to discrepancies between the approximated and true values.

Furthermore, the limitations on the stabilizing control inputs were modeled simplistically. For example, consider the limitations on the stepping performance of the model. Stepping speed was constrained by enforcing a constant minimum step time, independent of the step location. Step location was constrained by limiting the maximum step length, irrespective of the current CoM position or direction of motion. The expressions for capturability in this paper rely strongly on these simplistically modeled limitations.

We see an advantage in the simplicity of the presented models however. Comparable studies demonstrated that making the models even slightly more complex can result in expressions that are less comprehensible and require numerical methods to be solved (Wight et al. 2008; Pratt and Drakunov 2007). This decreases understanding and increases the computational burden. Although the models are very elementary, they are still useful for the analysis and control of legged locomotion.

9.2. Robustness metrics

We introduced the N-step capturability margin, which expresses the level of capturability for a single state and takes both the position and velocity of the CoM into account. Human subject studies already demonstrated that the CoM position and velocity in relation to the base of support is a good indicator of the ability to maintain balance and the number of steps required to do so (Pai and Patton 1997; Pai et al. 1998; Maki and McIlroy 1999; Hsiao and Robinovitch 2001; Aftab et al. 2010). Hof et al. (2005) were the first to formally define the distance between the instantaneous capture point (which these authors call the 'extrapolated CoM') and the base of support as a 'margin of stability'. We see an advantage to using our metrics, since they take the effects and limits of the stabilizing control inputs (foot placement, ankle torque and hip torque) into account.

9.3. More complex models

Although we were able to perform a complete capturability analysis for three simple models, it remains an open issue to find a more generally applicable analytical method, or even a numerical algorithm. A possible numerical algorithm could start with a small set of states that are known to be captured, such as default standing positions. This set can then be expanded by finding initial states in its neighborhood for which there exist evolutions that reach the set and contain no steps. Subsequently, sets of N-step capturable states can be found recursively by searching for states from which it is possible to reach an $(N-1)$-step capturable state in a single step. While this algorithm is conceptually simple, it is likely computationally prohibitive for a complex system. In addition, including the full state of the system requires knowledge of all relevant environment information, such as the ground profile and contact characteristics. Encoding the entire environment for all time is prohibitive in general. Also note that for a system with regions of chaotic dynamics, the capturability may be uncomputable, as determining whether a state is in an N-step viable-capture basin may be undecidable (Sipser 2005).

9.4. Capturability for a specific control system

The capturability analysis presented in this part took both the dynamics and actuation limits of the legged system into account, while no specific control law was assumed *a priori*. This approach allows us to make some strong conclusions concerning capturability. For example, if there is no ∞-step capture region, then it is impossible to make the legged system come to a stop without falling, no matter what control law is used. Another approach could be to assume an existing controller and determine capturability given that controller. We can also assume a partial controller, such as one that provides balance and swing leg control and takes a target step location as an input. Such a controller might have internal state, which must be incorporated into the robot state $\mathbf{x}$, but the range of actuator inputs to consider can be reduced, simplifying capturability analysis of the partially controlled system. We have used this approach to greatly reduce the actuation dimensionality of a lower body humanoid, admitting a machine learning solution for finding 1-step capture regions in simulation (Rebula et al. 2007). We also use such a parameterized controller for the robot in Part 2.

9.5. Capturability and viability

Preventing a fall is important for legged locomotion. A maximally robust control system would prevent falls for all states in which preventing a fall is possible. However, designing such a control system may be impractical. Instead, we design stabilizing control systems using techniques and analysis tools which prevent falls for a subset of the theoretically possible states. We believe that focusing on

preventing falls over a set of N-step capturable states will lead to robust control systems and that as N increases the states which are subsequently considered become less and less common and relevant. In addition, it is likely that analysis and control is computationally less complex for small N than for large N.

We hypothesize that nearly all human legged locomotion takes place in a 3-step viable capture basin and that all 3D bipedal robot locomotion demonstrated to date likely falls in a 2-step viable capture basin. Considering N-step capturability instead of viability focuses on the states from which it is the least difficult to avoid a fall. For large N, it may be best to just take the fall and switch to an emergency falling controller to protect the legged system and surrounding environment.

9.6. Future work

While the simple gait models presented in this part all pertain to bipedal walking, the concepts introduced in this paper can be applied to a wide range of walking and running legged systems, with any number of legs. One main area of future work is to generate walking and running models of increased complexity, develop algorithms for determining their capturability, and use the results to improve the robustness of legged robots. For humanoid walking robots, we are currently investigating models that incorporate uneven terrain, and consider the use of arms for pushing on walls and grabbing handrails in order to increase robustness.

10. Conclusion

In this paper we have introduced and defined N-step capturability, and demonstrated capturability analysis on three simple gait models. The main strength of capturability analysis lies in the explicit focus on avoiding a fall in a global sense, while considering the computationally simpler issue of the ability to come to a stop in a given number of steps.

By projecting N-step capturable states to the ground using contact reference points, we can generate capture regions which define appropriate foot placement, explicitly providing practical control information and leading to the N-step capturability margin, a useful robustness metric.

In Part 2 we show that the exact solutions to the simple models in this part can be successfully used as approximations for control of a lower-body humanoid.

Notes

1. All dimensionless quantities will be marked with a prime.
2. A point that cannot be reached can never be an N-step capture point.
3. Note that the ankle location is still used as the reference point for determining step length.
4. To be precise, $\mathbf{r}_{\mathrm{CoP}}$ is the foot rotation indicator (Goswami 1999), which must be kept inside the base of support to prevent foot rotation. If it is inside the base of support, then the CoP coincides with the foot rotation indicator; hence, we have chosen the notation $\mathbf{r}_{\mathrm{CoP}}$.
5. The equivalent constant CoP is only equivalent in terms of instantaneous capture point motion and not necessarily in terms of other parts of the state.
6. Informally speaking, the foot is optimally oriented when the toes point in the direction of the instantaneous capture point. See Figure 8.

Funding

This work was funded through the Army Tank and Automotive Research and Development Command (grant number W56HZV-04-C-0072), the Defense Advanced Research Projects Agency (grant number FA8650-05-C-7265), the Office of Naval Research (grant number N00014-09-1-0913-01), NASA (grant number NNX10AG54A), and the Honda Research Institute.

Acknowledgment

The authors gratefully acknowledge helpful discussions with D Karssen, whose ideas contributed to the work. We would like to thank E Westervelt for his helpful comments. Several anonymous reviewers also made helpful suggestions which improved the clarity of the paper.

References

Abdallah M and Goswami A (2005) A biomechanically motivated two-phase strategy for biped upright balance control. In *Proceedings of the 2005 IEEE International Conference on Robotics and Automation*. Piscataway, NJ: IEEE Press, pp. 1996–2001.

Aftab Z, Wieber P-B and Robert T (2010) Comparison of capture point estimation with human foot placement: applicability and limitations. Oral presentation at *5èmes Journées Nationales de la Robotique Humanoïde*.

Aubin J-P (1991) *Viability theory*. Boston, MA: Birkhäuser.

Aubin J-P, Lygeros J, Quincampoix M, Sastry S and Seube N (2002) Impulse differential inclusions: a viability approach to hybrid systems. *IEEE Transactions on Automatic Control* 47: 2–20.

Byl K and Tedrake R (2008) Metastable walking on stochastically rough terrain. In *Proceedings of Robotics: Science and Systems IV*, Zurich, Switzerland.

Chevallereau C, Abba G, Aoustin Y, et al. (2003) RABBIT: a testbed for advanced control theory. *IEEE Control Systems Magazine* 23(5): 57–79.

Coleman MJ, Garcia M, Mombaur K and Ruina A (2001) Prediction of stable walking for a toy that cannot stand. *Physical Review E* 64(2): 022901.

Dingwell JB, Cusumano JP, Cavanagh P and Sternad D (2001) Local dynamic stability versus kinematic variability of continuous overground and treadmill walking. *Journal of Biomechanical Engineering* 123: 27–32.

Englsberger J, Ott C, Roa M, Albu-Schäffer A and Hirzinger G (2011) Bipedal walking control based on capture point dynamics. In *Proceedings of the 2011 IEEE/RSJ International Conference on Intelligent Robotic Systems*

Forner Cordero A, Koopman H and van der Helm F (2003) Multiple-step strategies to recover from stumbling perturbations. *Gait and Posture* 18: 47–59.

Goswami A (1999) Postural stability of biped robots and the foot rotation indicator (FRI) point. *The International Journal of Robotics Research* 18: 523–533.

Guihard M and Gorce P (2002) Dynamic control of bipeds using ankle and hip strategies. In *Proceedings of the 2002 IEEE/RSJ International Conference on Intelligent Robotic Systems*, vol. 3.

Hobbelen DGE and Wisse M (2007a). A disturbance rejection measure for limit cycle walkers: the gait sensitivity norm. *IEEE Transactions on Robotics* 23: 1213–1224.

Hobbelen DGE and Wisse M (2007b) Limit cycle walking. In Hackel M (ed.), *Humanoid Robots, Human-like Machines*. Vienna: ITech Education and Publishing, pp. 277–294.

Hof AL (2008) The 'extrapolated center of mass' concept suggests a simple control of balance in walking. *Human Movement Science* 27: 112–125.

Hof AL, Gazendam M and Sinke W (2005) The condition for dynamic stability. *Journal of Biomechanics* 38: 1–8.

Hof AL, van Bockel RM, Schoppen T and Postema K (2007) Control of lateral balance in walking: Experimental findings in normal subjects and above-knee amputees. *Gait and Posture* 25: 250–258.

Hof AL, Vermerris SM and Gjaltema WA (2010) Balance responses to lateral perturbations in human treadmill walking. *Journal of Experimental Biology* 213: 2655–2664.

Horak F and Nashner L (1986) Central programming of postural movements: adaptation to altered support-surface configurations. *Journal of Neurophysiology* 55: 1369.

Hsiao ET and Robinovitch SN (2001) Elderly subjects' ability to recover balance with a single backward step associates with body configuration at step contact. *Journal of Gerontology A: Biological Science and Medical Science* 56(1): M42–M47.

Hsiao-Wecksler ET and Robinovitch SN (2007) The effect of step length on young and elderly women's ability to recover balance. *Clinical Biomechanics* 22: 574–580.

Hyon S-H, Hale J and Cheng G (2007) Full-body compliant human–humanoid interaction: balancing in the presence of unknown external forces. *IEEE Transactions on Robotics* 23: 884–898.

Kajita S, Kanehiro F, Kaneko K, Yokoi K and Hirukawa H (2001) The 3D Linear Inverted Pendulum Model: A simple modeling for a biped walking pattern generation. In *Proceedings of the 2001 IEEE/RSJ International Conference on Intelligent Robotic Systems*, vol. 1, pp. 239–246.

Kajita S and Tanie K (1991) Study of dynamic biped locomotion on rugged terrain—derivation and application of the linear inverted pendulum mode. In *Proceedings of the 1991 IEEE International Conference on Robotics and Automation*, vol. 2. Los Alamitos, CA: IEEE Computer Society Press, pp. 1405–1411.

Lee S-H and Goswami A (2007) Reaction mass pendulum (RMP): An explicit model for centroidal angular momentum of humanoid robots. In *Proceedings of the IEEE International Conference on Robotics and Automation*. Piscataway, NJ: IEEE, pp. 4667–4672.

Maki BE and McIlroy WE (1999) The control of foot placement during compensatory stepping reactions: does speed of response take precedence over stability? *IEEE Transactions on Rehabilitation Engineering* 7: 80–90.

Manchester IR, Mettin U, Iida F and Tedrake R (2009) Stable dynamic walking over rough terrain: Theory and experiment. In *Proceedings of the International Symposium on Robotics Research*

Masani K, Vette AH and Popovic MR (2006) Controlling balance during quiet standing: Proportional and derivative controller generates preceding motor command to body sway position observed in experiments. *Gait and Posture* 23: 164–172.

McGeer T (1990) Passive walking with knees. In *Proceedings of the 1990 IEEE International Conference on Robotics and Automation*, Cincinnati, OH, pp. 1640–1645.

Millard M, Wight DL, McPhee J, Kubica EG and Wang DW (2009) Human foot placement and balance in the sagittal plane. *Journal of Biomechanical Engineering* 131(12): 121001.

Morimoto J, Nakanishi J, Endo G, Cheng G, Atkeson CG and Zeglin G (2005) Poincaré-map-based reinforcement learning for biped walking. In *Proceedings of the 2005 IEEE International Conference on Robotics and Automation*. Piscataway, NJ: IEEE Press, pp. 2381–2386.

Morisawa M, Harada K, Kajita S, et al. (2009) Reactive stepping to prevent falling for humanoids. In *2009 IEEE-RAS International Conference on Humanoid Robotics*. Piscataway, NJ: IEEE Press, pp. 528–534.

Nenchev DN and Nishio A (2008) Ankle and hip strategies for balance recovery of a biped subjected to an impact. *Robotica* 26: 643–653.

Nishiwaki K and Kagami S (2010) Strategies for adjusting the ZMP reference trajectory for maintaining balance in humanoid walking. In *Proceedings of the 2010 IEEE International Conference on Robotics and Automation*, pp. 4230–4236.

Okumura Y, Tawara T, Endo K, Furuta T and Shimizu M (2003) Realtime ZMP compensation for biped walking robot using adaptive inertia force control. In *Proceedings of the 2003 IEEE/RSJ International Conference on Intelligent Robotic Systems*, vol. 1, pp. 335–339.

Orin DE and Goswami A (2008) Centroidal momentum matrix of a humanoid robot: structure and properties. In *Proceedings of the 2008 IEEE/RSJ International Conference on Intelligent Robotic Systems*, pp. 653–659.

Pai Y-C and Patton J (1997) Center of mass velocity–position predictions for balance control. *Journal of Biomechanics* 30: 347–354.

Pai Y-C, Rogers MW, Patton J, Cain TD and Hanke TA (1998) Static versus dynamic predictions of protective stepping following waist-pull perturbations in young and older adults. *Journal of Biomechanics* 31: 1111–1118.

Pavol MJ, Owings TM, Foley KT and Grabiner MD (2000) Mechanisms leading to a fall from an induced trip in healthy older adults. *Journal of Gerontology A: Biological Science and Medical Science* 56(7): M428–M437.

Pijnappels M, Kingma I, Wezenberg D, Reurink G and van Dieën J (2010) Armed against falls: the contribution of arm movements to balance recovery after tripping. *Experimental Brain Research* 201: 689–699.

Popovic MB, Goswami A and Herr HM (2005) Ground reference points in legged locomotion: definitions, biological trajectories and control implications. *The International Journal of Robotics Research* 24: 1013–1032.

Pratt JE, Carff J, Drakunov SV and Goswami A (2006) Capture point: a step toward humanoid push recovery. In *Proceedings of the 2006 IEEE-RAS International Conference on Humanoid Robotics*. Piscataway, NJ: IEEE Press, pp. 200–207.

Pratt JE and Drakunov SV (2007) Derivation and application of a conserved orbital energy for the inverted pendulum bipedal walking model. In *Proceedings of the 2007 IEEE International Conference on Robotics and Automation*

Pratt JE and Krupp BT (2008) Design of a bipedal walking robot. In *Proceedings of SPIE* 6962.

Pratt JE and Tedrake R (2006) Velocity-based stability margins for fast bipedal walking. In Diehl M and Mombaur K (eds), *Fast Motions in Biomechanics and Robotics* (*Lecture Notes in Control and Information Sciences*, volume 340). Berline: Springer, pp. 299–324.

Pratt JE, Koolen T, de Boer T, Rebula J, Cotton S, Carff J, Johnson M and Neuhaus P (2012) Capturability-based analysis and control of legged locomotion, Part 2: Application to M2V2, a lower-body humanoid. *The International Journal of Robotics Research*, in press.

Rebula JR, Cañas F, Pratt JE and Goswami A (2007) Learning capture points for humanoid push recovery. In *Proceedings of the 2007 IEEE-RAS International Conference on Humanoid Robotics.*

Roos PE, McGuigan MP, Kerwin DG and Trewartha G (2008) The role of arm movement in early trip recovery in younger and older adults. *Gait and Posture* 27: 352–356.

Sipser M (2005) *Introduction to the Theory of Computation*. Course Technology.

Smeesters C, Hayes W and McMahon T (2001) The threshold trip duration for which recovery is no longer possible is associated with strength and reaction time. *Journal of Biomechanics* 34: 589–595.

Stephens BJ (2007a) Humanoid push recovery. In *Proceedings of the 2007 IEEE-RAS International Conference on Humanoid Robotics*. Piscataway, NJ: IEEE Press, pp. 589–595.

Stephens BJ (2007b) Integral control of humanoid balance. In *Proceedings of the 2007 IEEE/RSJ International Conference on Intelligent Robotic Systems*. Piscataway, NJ: IEEE Press, pp. 4020–4027.

Takenaka T, Matsumoto T and Yoshiike T (2009) Real time motion generation and control for biped robot - 1st report: Walking gait pattern generation. In *Proceedings of the 2009 IEEE/RSJ International Conference on Intelligent Robotic Systems*. Piscataway, NJ: IEEE Press, pp. 1084–1091.

Thelen DG, Wojcik LA, Schultz AB, Ashton-Miller JA and Alexander NB (1997) Age differences in using a rapid step to regain balance during a forward fall. *Journal of Gerontology A: Biological Science and Medical Science* 52(1): M8–M13.

Townsend MA (1985) Biped gait stabilization via foot placement. *Journal of Biomechanics* 18: 21–38.

van der Burg J, Pijnappels M and van Dieën J (2005) Out-of-plane trunk movements and trunk muscle activity after a trip during walking. *Experimental Brain Research* 165: 407–412.

Vukobratovic M and Stepanenko J (1972) On the stability of anthropomorphic systems. *Mathematical Biosciences* 15: 1–37.

Weerdesteyn V, Nienhuis B, Mulder T and Duysens J (2005) Older women strongly prefer stride lengthening to shortening in avoiding obstacles. *Experimental Brain Research* 161: 39–46.

Wieber P-B (2000) Constrained dynamics and parametrized control in biped walking. In *International Symposium on the Mathematics of Theoretical Network Systems*. Perpignan: SIAM.

Wieber P-B (2002) On the stability of walking systems. In *Proceedings of the International Workshop on Humanoid and Human Friendly Robotics*, Tsukuba, Japan, pp. 53–59.

Wight DL, Kubica EG and Wang DW (2008) Introduction of the foot placement estimator: a dynamic measure of balance for bipedal robotics. *Journal of Computational and Nonlinear Dynamics* 3(1): 011009.

Winter DA (1990) *Biomechanics and Motor Control of Human Movement* (2nd edn). New York: John Wiley & Sons.

Wojcik LA, Thelen DG, Schultz AB, Ashton-Miller JA and Alexander NB (2001) Age and gender differences in peak lower extremity joint torques and ranges of motion used during single-step balance recovery from a forward fall. *Journal of Biomechanics* 34: 67–73.

Yin K, Loken K and van de Panne M (2007) SIMBICON: simple biped locomotion control. In *Proceedings of the SIGGRAPH 2010*. New York: ACM Press, p. 105.

Appendix A: Anthropomorphic model parameters

We estimated anthropomorphic model parameters for the 3D-LIPM with finite-sized foot and reaction mass, see Table A1. Mass and length parameters are based on a typical human 1.75 m tall and with a mass of 70 kg. Gait parameters are based on experimental studies on human trip recovery.

Table A1. Estimates of anthropomorphic model parameters.

Parameter	Symbol	Value	Units	Reference
Step length	$l_{\max}$	0.7	m	Pavol et al. (2000) and Forner Cordero et al. (2003)
Minimum step time	Δt_s	0.3	s	Pavol et al. (2000) and Forner Cordero et al. (2003)
Ankle to toe length	$r_{\max}$	0.2	m	Winter(1990)
CoM height	z_0	0.95	m	Winter(1990)
HAT segment max. angle	$\theta_{\max}$	0.5	rad	Pavol et al. (2000) and vanderBurg et al. (2005)
Moment of inertia of HAT w.r.t. body CoM	J	8	kg m^2	Winter (1990)
Body mass	m	70	kg	Winter (1990)
Hip torque	$\tau_{\text{hip,max}}$	100	Nm	Wojcik et al. (2001)

Appendix B: Index to Multimedia Extensions

The multimedia extension page is found at http://www.ijrr.org

Table of Multimedia Extensions

Extension	Type	Description
1	Code	Matlab GUI demonstrating N-step capture regions.